Research article

Identification of cuproptosis-related miRNAs in triple-negative breast cancer and analysis of the miRNA–mRNA regulatory network

Yitao Wang [a], Jundan Wang [a], Jing Jiang [c], Wei Zhang [c], Long Sun [c], Qidong Ge [c], Chao Li [c], Xinlin Li [c], Xujun Li [c], Shenghong Shi [a,b,c,*]

[a] Health Science Center, Ningbo University, Ningbo, 315211, China
[b] Department of Oncology, Ningbo No.2 Hospital, Ningbo, 315010, China
[c] Department of Breast Surgery, Ningbo No.2 Hospital, Ningbo, 315010, China

ARTICLE INFO

ABSTRACT

Introduction: The close association between cuproptosis and tumor immunity in triple-negative breast cancer (TNBC) allows its monitoring for predicting the prognosis of patients with TNBC. Nevertheless, the biological function and prognostic value of cuproptosis-related miRNAs and their target genes have not been reported.

Purpose: To construct the miRNA and mRNA-based risk models associated with cuproptosis for patients with TNBC.

Methods: Comparison of expression levels for genes associated with cuproptosis was executed between patients in the normal individuals and the TCGA-TNBC cohort. Conducting differential analysis resulted in the identification of differentially expressed miRNA (DE-miRNAs) and differentially expressed genes (DEGs) between the TNBC and Control samples. Screening for prognostic miRNAs and biomarkers involved employing univariate Cox analysis and least absolute shrinkage and selection operator regression analyses. These methods were utilized to construct risk models aimed at predicting the survival of patients with TNBC. Based on the median value of risk scores, patients were then stratified into low- and high-risk groups. Functional enrichment analysis was employed to explore the potential function and pathways of prognostic genes. Additionally, independent prognostic analysis was performed through univariate and multivariate Cox regression. Immune infiltration analysis was performed to examine disparities in the infiltration of immune cells between the two risk groups. Finally, the prognostic gene expression was mined in key cell types of TNBC.

Results: We obtained 5213 DEGs and 204 DE-miRNAs related to cuproptosis between TNBC and Control samples. Five prognostic miRNAs (miR-203a-3p, miR-1277–3p, miR-135b-5p, miR-200c-3p, and miR-592) and three biomarkers (DENND5B, IGF1R, and MEF2C) were closely associated with TNBC. Significant differences in the functions of prognostic genes between the two risk groups were observed, encompassing adipogenesis, inflammatory response, and hormone metabolic process. The prognostic gene regulatory network revealed that miR200C-3p regulated ZFPM2 and CFL2, and miR-1277–3p regulated BMP2 and RORA. A nomogram was created based on riskScore, cancer status, and pathologic stage to predict 1/3/5-year survival of patients with TNBC. Immune infiltration analysis indicated that the immune microenvironment may be

---

* Corresponding author. Department of Breast Surgery, Ningbo No.2 Hospital, 41 Xibei Street Road, Ningbo, 315010, China.
 *E-mail address:* shishenghong@nbu.edu.cn (S. Shi).

associated with the progression of TNBC. Interestingly, prognostic genes exhibited higher expression levels in T cells, fibroblasts, endothelial cells, and monocytes compared to other cells. *Conclusions:* Five prognostic miRNA (miR-203a-3p, miR-1277–3p, miR-135b-5p, miR-200c-3p, and miR-592) and three biomarkers (DENND5B, IGF1R, and MEF2C) were significantly associated with TNBC, it provides new therapeutic targets for the treatment and prognosis of TNBC.

Simple Summary: Cuproptosis is closely related to tumor immunity in triple-negative breast cancer (TNBC). Analyzing the expression of genes associated with cuproptosis, we identified 5213 genes and 204 miRNAs with differential expression in TNBC and control samples using differential analysis. The prognostic miRNAs and biomarkers were screened using single factor Cox proportional risk and least absolute shrinkage and selection operator regression analyses. The analysis of immune infiltration was conducted to examine variations in the infiltration of immune cells within low- and high-risk populations. Five prognostic miRNAs and three biomarkers were closely associated with TNBC. Therefore, potential therapeutic targets for TNBC encompass cuproptosis-related miRNAs and their regulatory target genes.

1. Introduction

Breast cancer is the primary contributor to cancer-related morbidity, disability, and mortality in women worldwide. As of the year 2020, it remained the most prevalent malignancy in terms of incidence [1]. Breast cancer subtypes are delineated based on histopathologic characteristics and the absence or presence of specific molecular markers, including human epidermal growth factor receptor 2 (HER2; also referred to as ERBB2), progesterone receptor (PR), and estrogen receptor (ER). However, a therapeutic challenge persists in roughly 10%–20% of breast cancer cases where there is a negative expression for HER2, PR, and ER. This specific subtype of breast cancer is commonly denoted as triple-negative breast cancer (TNBC), characterized by a lack of well-defined molecular markers. It is linked to an aggressive clinical course, characterized by poor overall survival (OS) and a short progression-free survival. Patients with TNBC show a median time to death of approximately 4.2 years and a median survival of 10 years after diagnosis. In contrast, patients with other subtypes of breast cancer show time to death and survival of 6 and 18 years, respectively [2,3]. Studies on the progression of TNBC are limited; therefore, investigating the underlying mechanism is essential. The rapid development of molecular biological information technology makes the research on breast cancer break through to the molecular level and discuss the effective targets of breast cancer proliferation and metastasis, which will lay an important foundation for the future breast cancer diagnosis and treatment [4].

MicroRNAs (miRNAs) are small, noncoding, and single-stranded RNAs pivotal in the regulation of gene expression, and they hold significance in the context of TNBC tumors. The biological behavior of TNBC cells is modulated by miR-543, which directly targets the
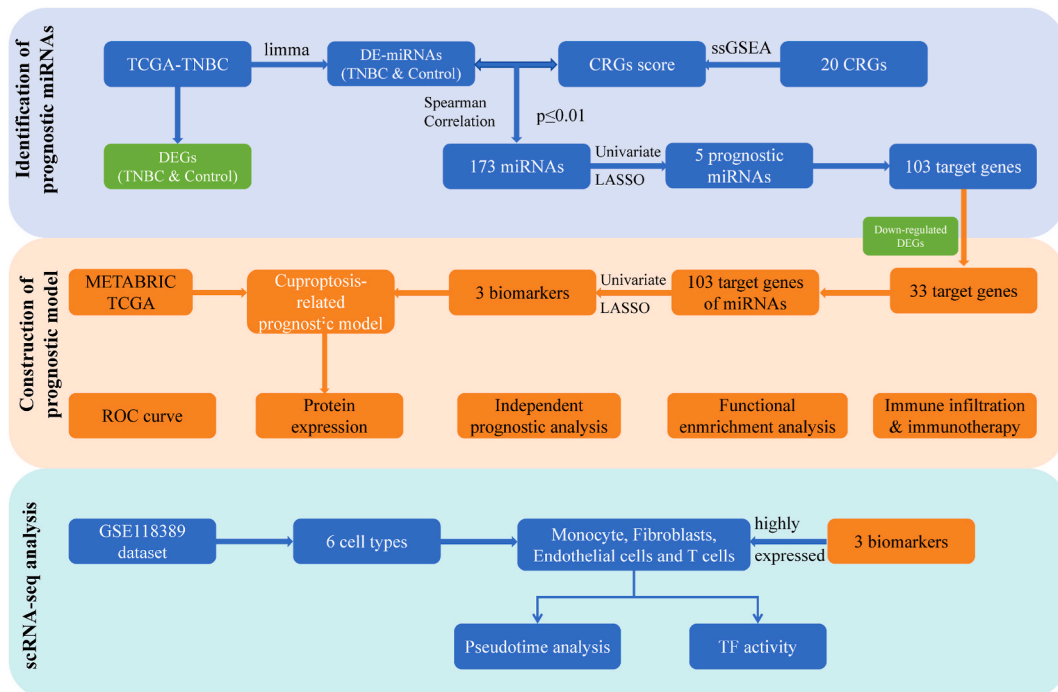
Fig. 1. Workflow to explore the prognostic value of cuproptosis-related miRNAs in TNBC.

ACTL6A gene. Therefore, it can be targeted for both diagnostic and therapeutic interventions for TNBC [5]. MiR-211–5p acts as a tumor suppressor in the progression of TNBC by targeting the SETBP1 gene, indicating its prognostic and therapeutic potential for TNBC [6].

Copper, an indispensable trace element, is requisite for numerous biological processes [7]. Cuproptosis, a distinctive and novel mode of cell death, relies on copper and specific miRNAs. It occurs when copper binds to lipoylated enzymes within the tricarboxylic acid cycle and triggers protein aggregation and proteotoxic stress, ultimately leading to cell death [8]. The influence of cuproptosis-related genes (CRGs) on the clinicopathologic characteristics and prognosis of TNBC has been documented. CRGs exhibit a close association with tumor immunity in TNBC and can serve as predictive markers for patient prognosis [9]. Current research endeavors have concentrated on exploring the potential prognostic significance of CRGs in TNBC, demonstrating a close correlation between CRGs and tumor immunity in TNBC [9–11]. However, miRNAs associated with TNBC have not been explored to date. Therefore, our study explored miRNAs associated with TNBC prognosis and their target genes to construct prognosis prediction models.

This study employed least absolute shrinkage and selection operator (LASSO) and univariate Cox regression analyses to obtain biomarkers. Subsequently, prognostic risk models were constructed and verified. Five prognostic miRNAs were obtained, namely MIMAT0000617, MIMAT0003260, MIMAT0000758, MIMAT0005933, and MIMAT0000264. In addition, a new prognostic model was established for patients with TNBC based on three prognostic genes, namely DENND5B, IGF1R, and MEF2C. Overall, our findings revealed new potential prognostic markers and therapeutic targets for TNBC. Fig. 1 depicts the flow chart of the study.

2. Materials and Methods

2.1. Date sources

Acquiring the RNA-sequencing (RNA-seq) data for TNBC involved accessing the data on mRNA and miRNA from The Cancer Genome Atlas (TCGA) database (https://portal.gdc.cancer.gov/). The mRNA dataset included 125 normal (Control) and 116 TNBC samples, and the miRNA dataset included 75 Control and 81 TNBC samples. In addition, the TCGA database yielded somatic mutation data for 97 samples of TNBC. In addition, 298 TNBC samples with complete survival information in the Molecular Taxonomy of Breast Cancer International Consortium (METABRIC) database (https://www.mercuriolab.umassmed.edu/metabric)were included in the training set. GSE38959, GSE157284, and GSE118389 datasets were acquired from the National Center for Biotechnology Information database (https://www.ncbi.nlm.nih.gov/geo/). Comprising 13 normal samples and 30 samples from individuals with TNBC, the RNA-seq dataset GSE38959 was utilized. The RNA-seq dataset GSE157284 included 82 patients with TNBC, and their clinical data included the results of PD-L1 immunohistochemistry. Single-cell RNA-seq (scRNA-seq) data of six primary TNBC tumors were included in the GSE118389 dataset. The dataset included 20 CRGs, namely MTF1, GLS, ATP7B, FDX1, LIAS, LIPT1, DLD, DLAT, CDKN2A, ATP7A, PDHB, PDHA1, GCSH, LIPT2, DLST, DBT, SLC31A1 (CTR1), NFE2L2, NLRP3, and CTR2 [12–15].

2.2. Analysis of CRGs in TNBC

To extract the mutation types of TNBC samples, the somatic mutation data from the TCGA-TNBC cohort underwent analysis through the maftools package (v 2.8.05) [16] to obtain the mutation types of TNBC samples. In addition, the mutation rates of genes in TNBC samples were analyzed. The location of CRGs on 24 chromosomes was determined using the RCircos (v 1.2.2) package [17]. Next, a univariate Cox analysis was executed to derive the risk value score for each CRG. Furthermore, a network of protein–protein interaction (PPI) involving these risk factors was established through the utilization of the STRING database (http://stringdb.org). The somatic mutation rates of CRGs in TNBC samples were analyzed, and their expressions were compared between patients with TNBC and Control samples. According to the CRG expression, patients were stratified into subgroups based on low and high levels. Subsequent comparison of the survival between these two subgroups was conducted, and Kaplan–Meier (K–M) survival curves were plotted.

2.3. Screening of differentially expressed genes (DEGs) and miRNAs

DEGs between 125 TNBC and 116 Control samples and differentially expressed miRNA (DE-miRNAs) between 75 TNBC and 81 Control samples of miRNA expression matrix were obtained using the limma (v 3.48.3) package (adj.p.value < 0.05& |log2FC| > 1) [18]. The generation of heat maps was accomplished utilizing the pheatmap package (v 1.0.12), while the volcano maps were plotted utilizing the ggplot2 package (v 3.3.5) [19]. The computation of the cuproptosis score for each patient with TNBC in the TCGA dataset involved applying the gene set variation analysis (GSVA; v 1.44.5) package and utilizing the single-sample gene set enrichment analysis (ssGSEA) algorithm. Correlations between the DE-miRNAs and the cuproptosis scores were computed utilizing the Spearman method (p.value ≤ 0.01). The candidate miRNAs were obtained based on the correlation values.

2.4. Screening of prognostic miRNAs

Candidate miRNA expression was used as a continuous variable, and univariate Cox proportional hazard regression analysis was conducted utilizing the survival (v 3.2–13) package [19] to obtain survival-related miRNAs (p.value < 0.05). Furthermore, survival-related miRNAs were analyzed with the LASSO algorithm using the glmnet (v 4.1–3) package to obtain prognostic miRNAs.

Following the classification based on the median value of the risk score, the samples were stratified into low- and high-risk groups.

Evaluation of the prognostic value of the risk model was conducted utilizing the TCGA miRNA dataset. The calculation of the risk score for each sample involved the utilization of the following formula: Riskscore = exp $(\beta 1X1 + \beta 2X2 + \dots + \beta nXn)$, of which X represents the miRNA expression, and β refers to the regression coefficient. The risk curve of the heat map and the risk model of miRNA expression were plotted. The K–M survival curve was drawn using the survminer (v 0.4.9) package, including disease-free and overall survival, for both the risk groups. Finally, the receiver operating characteristic (ROC) curves were plotted for 1–5-year OS. In addition, the ROC curves for each prognostic miRNA and the risk model were plotted to predict relapsed versus non-relapsed, survival, and death outcomes in patients with TNBC.

2.5. Enrichment analysis and the construction of a regulatory network

Hallmark enrichment and gene ontology (GO) analyses were conducted on samples within the two risk groups utilizing org. Hs.eg. db (v 3.13.0) and clusterProfiler (v 4.0.2) to delve deeper into potential biological mechanisms and relevant signaling pathways in these groups [20]. We predicted the downstream mRNAs of the prognostic miRNAs from the miRTarBase (http://miRTarBase.mbc. nctu.edu.tw/) miRWalk (http://mirwalk.uni-hd.de/), and miRDB (https://mirdb.org/) databases. The predicted outcomes from the three databases were intersected to obtain the regulatory mRNAs (target genes) of the prognostic miRNAs. Because the prognosis of miRNAs was significantly increased in patients, according to the theory of miRNA-mRNA, and significantly reduced genes in patients were selected to intersect with predicted target genes of miRNA. Furthermore, GO and Kyoto Encyclopedia of Genes and Genomes (KEGG) enrichment analyses were carried out utilizing clusterProfiler (v 3.14.3) [20] (p.adjust <0.05 and count ≥1) to explore associated signaling pathways and functions of target genes. Finally, the ClueGo plug-in within the Cytoscape software was employed to visualize the enrichment analysis of target genes.

2.6. Screening of biomarkers

The training set included 298 patients with TNBC in the METABRIC dataset with complete survival information. The external validation set comprised 80 patients in the TCGA-TNBC dataset with complete survival information. We then created a risk model for the training set using univariate Cox and LASSO regression analyses and validated the model in the validation set. In addition, univariate proportional hazard Cox and LASSO regression analyses were performed on the target genes to identify biomarkers. Based on the median risk score, samples in the METABRIC and TCGA datasets were stratified into high- and low-risk groups. The evaluation of the prognostic value of the risk model occurred in the METABRIC dataset and underwent validation in the TCGA dataset. The formula for calculating the risk score is included in section 2.4, where X is the expression of the biomarker. For the METABRIC and TCGA datasets, the ROC curves for 1–5-year survival, K–M survival curves, heat map of miRNA expression, and risk curve of the risk model were generated. Furthermore, the expression levels of biomarkers obtained using the regression analysis were analyzed in the TCGA and GSE38959 datasets. Finally, we downloaded the results of immunohistochemical analysis of the prognostic genes from the Human Protein Atlas database (https://www.proteinatlas.org/).

2.7. Independent prognostic analysis

We used ggalluvial (v 0.12.3) to map the Alluvial and show the relationship between clinical characteristics. We compared the prognosis of two risk groups of the TCGA dataset containing complete clinical information of 72 samples. Furthermore, riskScore, age, cancer status, and other clinicopathologic factors were incorporated into the risk model for univariate COX-independent prognostic analysis. Next, the factors with p. value < 0.05 obtained in the univariate Cox analysis were incorporated into the multivariate Cox analysis. A nomogram was created to forecast survival rates of patients with TNBC (1-, 3-, and 5-year survival) based on clinical factors (p.value < 0.05) obtained from the above analysis. Further, a calibration curve was constructed to validate the nomogram utilizing the aforementioned prediction model.

2.8. Functional enrichment and immune infiltration analyses

We downloaded the hallmark pathway gene set using the msigdbr (v 7.4.1) package and used it as the preset pathway to explore the pathways activated in the two risk groups. The ssGSEA score of each pathway was obtained using the GSVA (v 1.44.5) package. The limma package was used to compare the scores of biological signaling pathways in the two risk groups. In addition, the ssGSEA algorithm was used to compute the abundance percentage of infiltrating immune cells in each TCGA sample (based on 24 immune cell sets). Next, the Wilcoxon test was applied to analyze the disparities in immune cell infiltration between the two risk groups. Finally, the relationship between immune cells and riskScore was analyzed utilizing the Pearson method.

2.9. Significance of riskScore

The riskScore values of patients with TNBC in the GSE157284 dataset were computed, and the patients were classified into the groups of high and low risk levels based on the median riskScore. A comparison of the expression levels of immune checkpoint genes was conducted between the two risk groups. Immunophenscores (IPS) for patients with TNBC were obtained from The Cancer Immunome Atlas database (https://www.tcia.at/). IPS was based on the expression of suppressor cells, effector cells, MHC molecules,
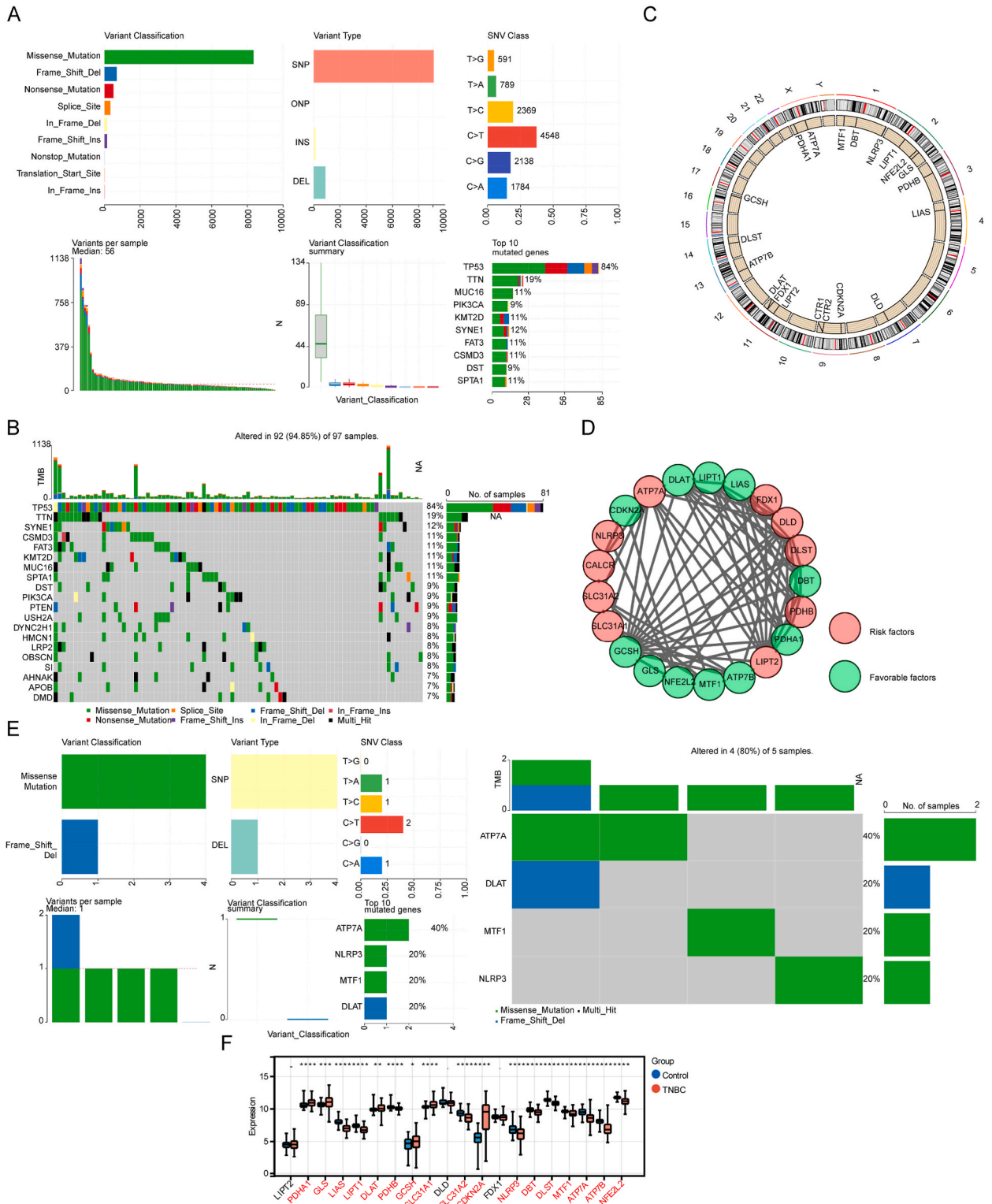
Fig. 2. Expression of CRGs in TNBC and the associated mutations. (A, B) Single nucleotide variation analysis of CRGs in TNBC. (C) Location of CRGs on 24 chromosomes. (D) PPI network showing risk and favorable factors. (E) Somatic mutation rates of CRGs in the TCGA-TNBC samples. (F) Comparative expressions of CRGs between TCGA-TNBC patients and Control samples. *p < 0.05, **p < 0.01, ***p < 0.001, and ****p < 0.0001.

and immunomodulators [21,22]. The Wilcoxon test was utilized to assess the differences in IPSs between the two risk groups. Chemotherapy is commonly used for the clinical treatment of malignant tumors; therefore, we used a predictive model to evaluate the drug sensitivity in the two risk groups using the Genomics of Drug Sensitivity in Cancer (GDSC) database (https://www.cancerrxgene.org/). The oncoPredict (v 0.2) package was used to assess the chemotherapy response in each patient based on the IC50 values. In addition, the chemotherapy response of patients in the two risk groups was determined (the list of drugs was sourced from the GDSC database). Specifically, IC50 values of four commonly used antibreast cancer drugs (5-fluorouracil, cisplatin, docetaxel, and paclitaxel) were obtained from the GDSC database and compared in the two risk groups.
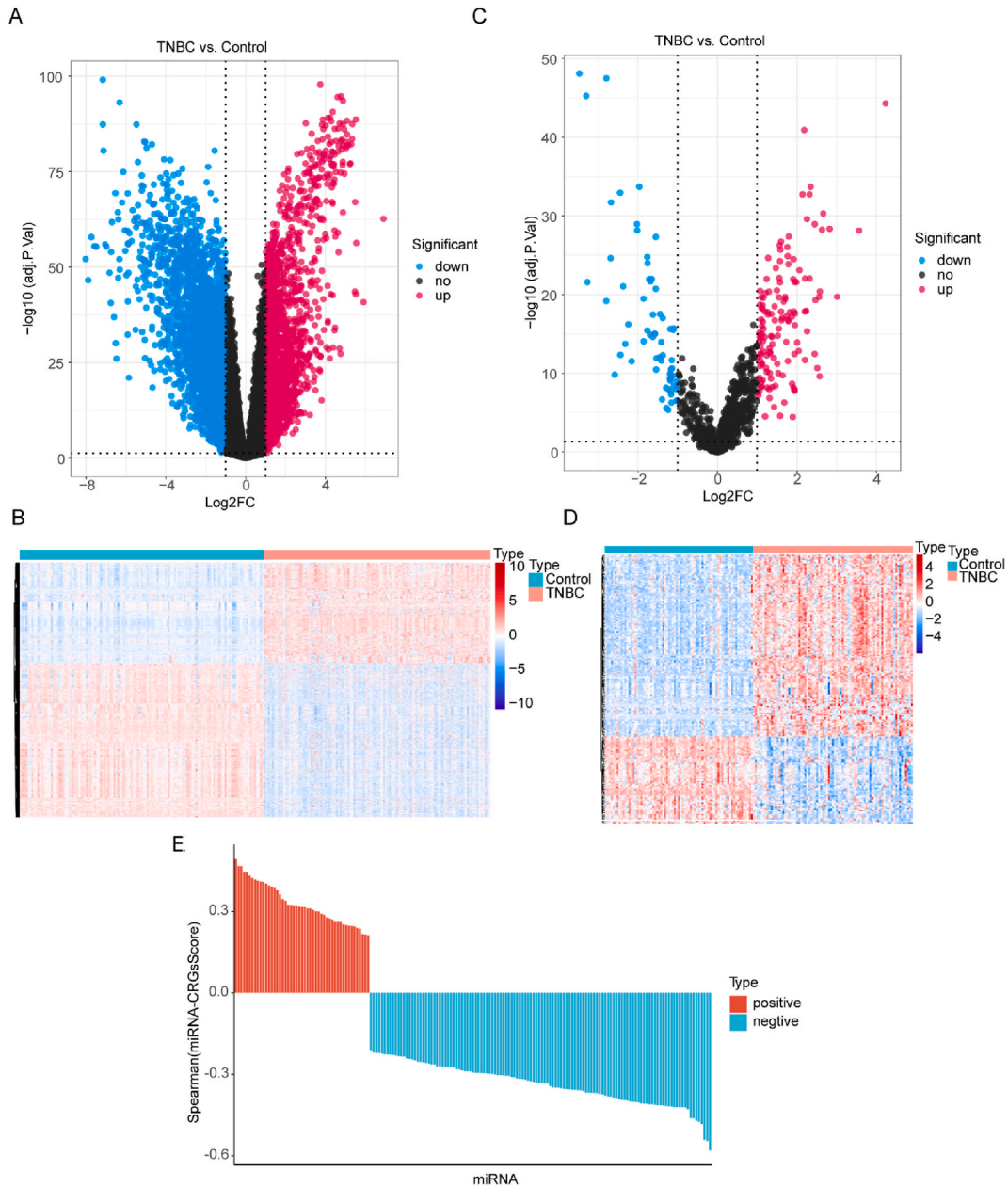

Fig. 3. DEGs and miRNAs. (A) Volcano plot of DEG expression between 125 TNBC and 116 Control samples; blue nodes denote downregulation, while red nodes signify upregulation. (B) Heat map for the expression levels of DEGs between the TNBC and Control samples. (C) Volcano plot of DE-miRNA expression between 75 TNBC and 81 Control samples. (D) Heat map for the expression levels of DE-miRNAs between TNBC and Control samples. (E) Candidate miRNAs identified using Spearman's correlation analysis (p.value $\leq$ 0.01). (For interpretation of the references to color in this figure legend, the reader is referred to the Web version of this article.)

2.10. Expression of cell subtypes and prognostic genes

We used Seurat (v 4.10) for quality control of the GSE118389 dataset (6 primary non-metastatic TNBC tumors). Genes that were detected in ≤3 low-quality cells, cells with ≥10% mitochondrial expression genes, and cells with a <200 count number of gene expression were excluded. We then reduced the dimension of the dataset and normalized the gene expression of the core cells using a linear regression model and performed the JackStraw and ScoreJackStraw functions to analyze available dimensions and determine whether the overall distribution of cells in each sample is consistent or there are significant outliers. Next, the tSNE algorithm was used to perform an overall dimensionality reduction analysis of the principal components with p < 0.05, and core cell clustering results were obtained. Furthermore, SingleR (v 1.6.1) was used to label different clusters in the Cellmarker database and identify each cell group. Based on the results of tSNE annotation, the analysis of the expression of prognostic genes in different cell types was conducted. The
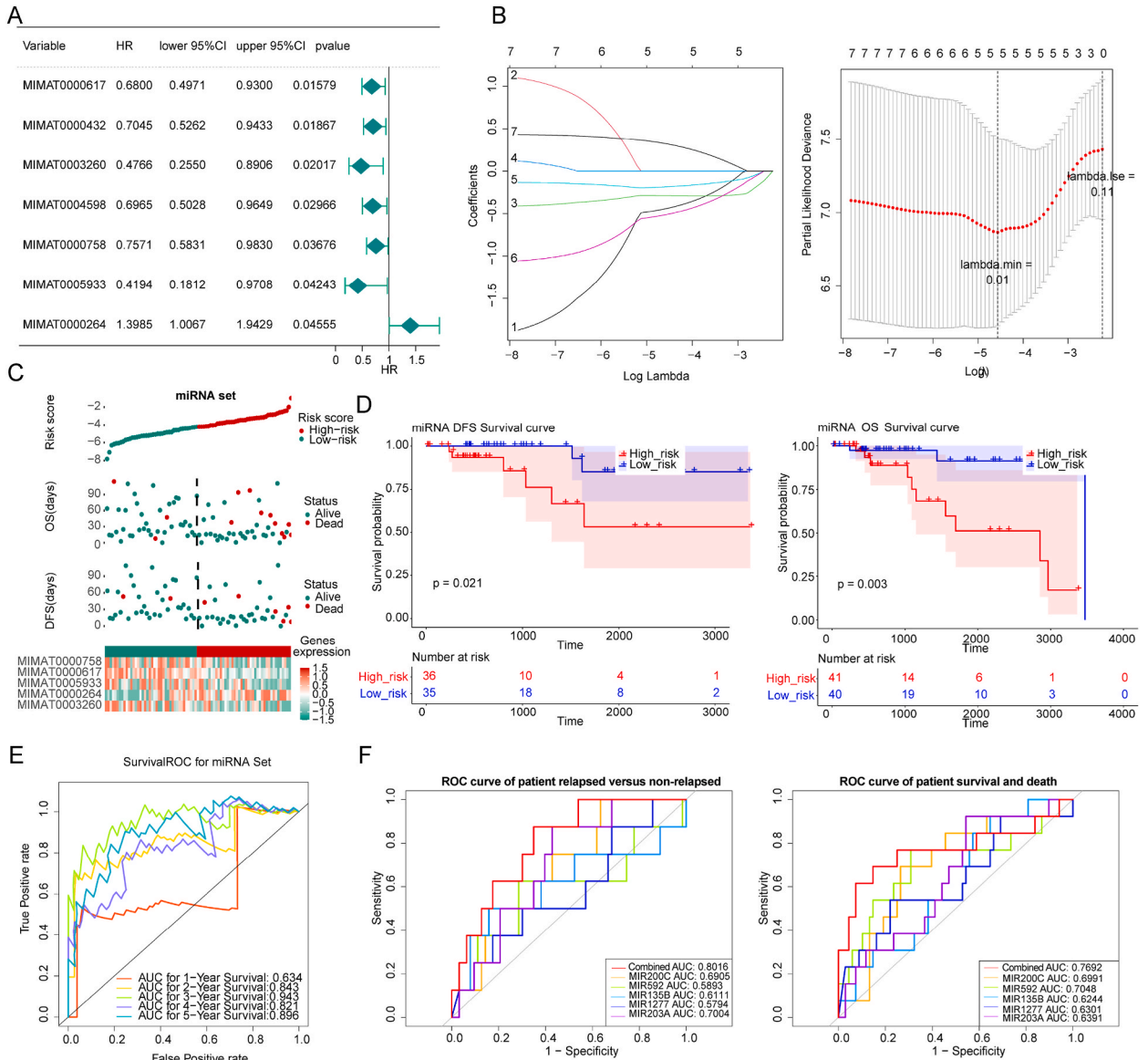
Fig. 4. Screening for prognostic miRNAs in TNBC. (A) Survival-related miRNAs obtained from candidate miRNAs using univariate Cox proportional hazard regression analysis. (B) Prognostic miRNAs obtained using the LASSO algorithm from the survival-related miRNAs. (C) Expression of prognostic miRNAs in the risk model. Heat map of the miRNA expression levels in the risk model. (D) K–M survival curves (including DFS and OS) for patients with TNBC having high/low-risk scores. (E) ROC curves for risk score models to predict 1–5-year OS in the TCGA miRNA dataset (The horizontal coordinate represents the false-positive rate and the vertical coordinate represents the true-positive rate. The larger the AUC of the ROC curve, the higher the accuracy of the prediction based on the model). (F) ROC curves of single prognostic miRNA to predict the status of the patient (relapsed versus non-relapsed, survival, and death).
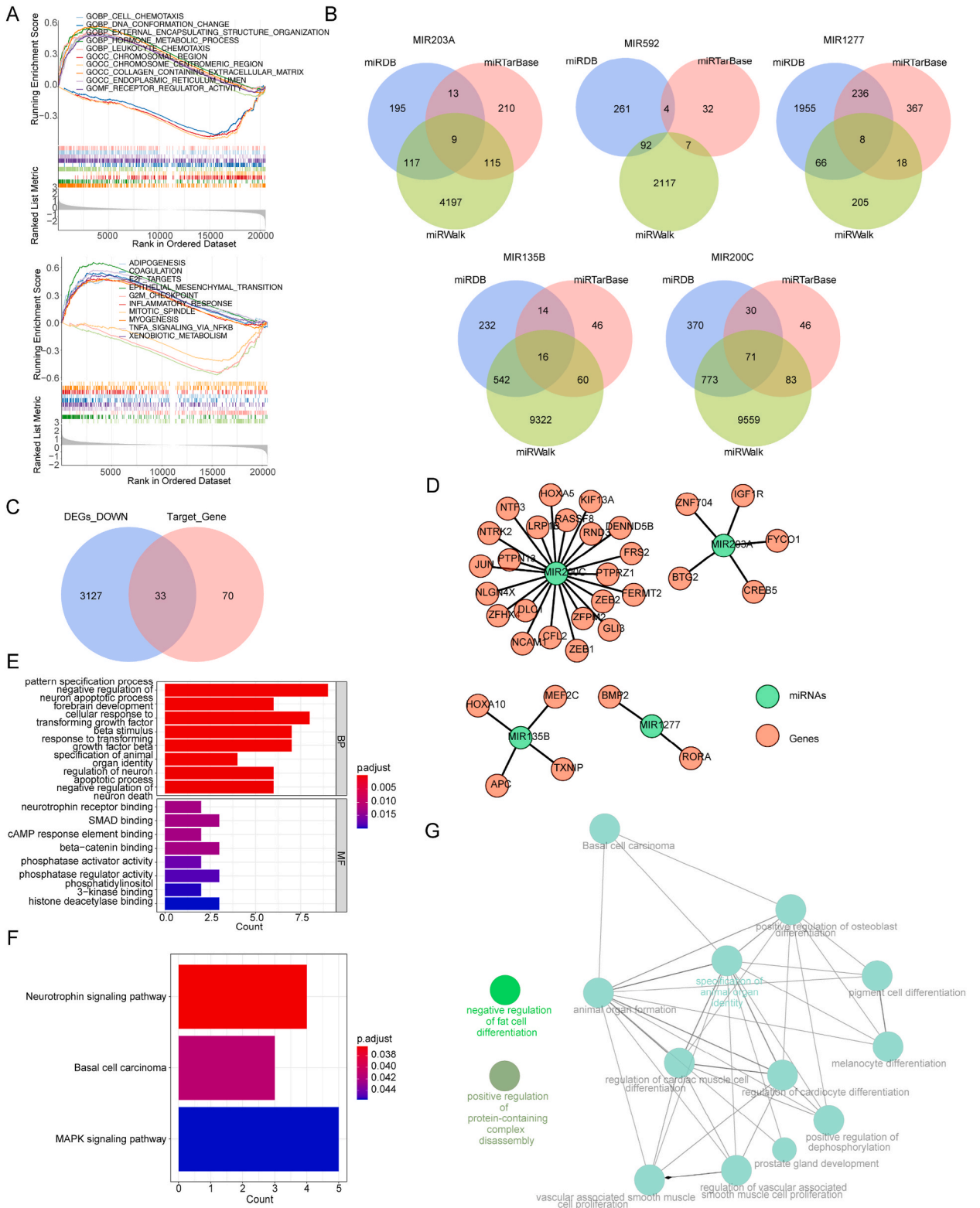
(caption on next page)

Fig. 5. Enrichment analysis and the miRNA–mRNA regulatory network. (A) GO and hallmark enrichment analysis in the two risk groups (The curves in the graph represent the running sum of the enrichment scores. The central portion of the graph delineates the position of genes associated with specific pathways, while the bottom part displays the distribution of the metric along with the list.) (B) Downstream regulatory genes of the prognostic miRNAs were predicted using miRDB, miRWalk, and miRTarBase. (C) Target genes of miRNAs based on the intersection of downregulated DEGs and target genes. (D) Construction of the PPI network of miRNA–mRNA. (E) GO enrichment analysis of target genes. (F) KEGG enrichment analysis of target genes. (G) Visualization of enrichment analysis of target genes using ClueGo.

Monocle 2 algorithm in the monocle (v 2.24.1) package was used for pseudotiming. Subsequently, the function "plot genes in pseudotime" of monocle (v 2.24.1) was performed to analyze the trajectory-dependent expression of biomarkers for linear differentiation. Finally, three types of regulators with high interaction confidence were selected using the dorothea (v 1.7.2) package. The TF activity of each cell was calculated based on the regulator, and the TF activity of the cell population was computed after the cells were reclustered according to the TF activity. Finally, the TFs with significant differences between different cell populations were compared.

3. Results

3.1. Expression of CRGs in TNBC and the associated mutations

We performed somatic mutation analysis to determine the genetic variation profile of CRGs in TNBC and found that most mutations were missense mutations (Fig. 2A). TP53 had the highest mutation rate in the TNBC samples (Fig. 2B). CRGs were located on chromosomes 1, 2, 3, 4, 7, 9, 11, 13, 14, 16, and X (Fig. 2C). Ten risk factors, including ATP7A and LIPT2, and 11 favorable factors, including GCSH and DLAT were observed in the PPI network (Fig. 2D). Four genes (ATP7A, DLAT, MTF1, and NLRP3) had missense mutations in four TNBC samples; however, the mutation frequency of CRGs in TNBC samples was low (Fig. 2E). Seventeen CRGs were significantly different between the TNBC and Control samples (Fig. 2F). The expression levels of GCSH, NLRP3, SLC31A2, and SLC31A1 exhibited significant correlations with the prognosis of the patients with TNBC (Supplementary F1igure 1). Overall, these results validated that cuproptosis was closely related to TNBC tumors.

3.2. Differential expression analysis

Overall, 5213 DEGs were discerned between TNBC and Control groups in the TCGA-TNBC cohort. Among these, 2053 exhibited upregulation, while 3160 displayed downregulation in the TNBC samples (Fig. 3A). The heat map illustrates the expression levels of DEGs between the TNBC and Control samples (Fig. 3B). In addition, 204 DE-miRNAs (138 upregulated and 66 downregulated) were identified between the TNBC and Control groups (Fig. 3C), and the heat map shows their expression levels (Fig. 3D). The calculation of cuproptosis scores for patients in the TCGA-TNBC dataset relied on the expression of CRGs (Supplementary T1able 1). Spearman's correlation analysis yielded 173 candidate miRNAs based on the p-value of ≤0.01 (Fig. 3E).

3.3. Identifying prognostic miRNAs

We obtained seven survival-related miRNAs, namely MIMAT0000758 (MIR135B), MIMAT0004598 (MIR141), MIMAT0000617 (MIR200C), MIMAT0000264 (MIR203A), MIMAT0005933 (MIR1277), MIMAT0000432 (MIR141), and MIMAT0003260 (MIR592) (Fig. 4A). LASSO regression analysis indicated five prognostic miRNAs (MIMAT0000617, MIMAT0003260, MIMAT0000758, MIMAT0005933, and MIMAT0000264) (Fig. 4B). The expression of MIMAT0000264 exhibited higher levels in the high-risk group (HR > 1) in contrast to the low-risk group. The expression of the remaining four miRNAs (MIMAT0000617, MIMAT0003260, MIMAT0000758, and MIMAT0005933) was higher in the low-risk group in contrast to the high-risk group (Fig. 4C). Significant differences in patient prognosis were observed between the two risk groups, with the high-risk group displaying a poorer prognosis (Fig. 4D). Notably, the 1–5-year AUC values were greater than 0.6 (Fig. 4E). Moreover, the AUC values (relapse and non-relapse, survival, and death) of the risk model were greater than 0.7, indicating the robust predictive capability of the model (Fig. 4F).

3.4. Enrichment analysis and the miRNA–mRNA regulatory network

GSEA indicated that samples in the two risk groups had significant differences in adipogenesis, inflammatory response, hormone metabolic process, and other functions (Fig. 5A). MIR135B had 16 downstream regulatory mRNAs, and MIR200C had 71 downstream regulatory mRNAs. Nine downstream regulatory mRNAs were screened for MIR203A, and MIR1277 had 8 downstream regulatory mRNAs. We obtained 103 target genes (mRNAs) after removing duplicate genes (Fig. 5B). The intersection of 3160 downregulated DEGs and 103 target genes revealed 33 target genes of miRNAs (Fig. 5C). MIR200C regulated ZFPM2 and CFL2, and BMP2 and RORA were regulated by MIR1277 (Fig. 5D). The GO enrichment analysis unveiled that 33 target genes of miRNAs were mainly linked to negative regulation of neuron death, negative regulation of neuron apoptotic process, and cellular response to transforming growth factor-beta stimulus (Fig. 5E). The KEGG enrichment analysis indicated that the target genes participated in the MAPK signaling pathway, basal cell carcinoma, and neurotrophin signaling pathway (Fig. 5F). Finally, ClueGo visualization indicated that the target genes were mainly associated with positive regulation of protein-containing complex disassembly and negative regulation of fat cell differentiation (Fig. 5G).

3.5. Identifying biomarkers

DENND5B, IGF1R, and MEF2C were the three survival-related genes (p.value < 0.05; Fig. 6A). The same three key genes (biomarkers) were identified using LASSO regression analysis (Fig. 6B). Moreover, these three biomarkers exhibited elevated expression levels in the low-risk group of the METABRIC dataset (Fig. 6C). The high-risk group demonstrated an unfavorable prognosis (Fig. 6D). AUC values surpassed 0.6, affirming the efficacy of the model (Fig. 6E). The biomarker expression patterns in the TCGA dataset were consistent with those in the METABRIC dataset (Fig. 7A–C). These biomarkers were significantly reduced in patients with TNBC in the TCGA and GSE38959 datasets (Fig. 7D–E). The immunohistochemical staining results of these biomarkers (downloaded from the Human Protein Atlas database) revealed that the expression of biomarkers was lower in patients with TNBC than in Control samples (Fig. 7F).

### 3.6. Independent prognostic analysis of the risk model

Supplementary F1igure 2Ashows the relationships between different clinical features The prognoses of patients with TNBC exhibited significant differences in the two risk groups, indicating the well-constructed nature of the model and its applicability to different clinical traits (Supplementary F1igure 2B). The p. values for cancer status, pathologic stage, pathologic T, and riskScore were less than 0.05 (Fig. 8A). Finally, cancer status, pathologic stage, and riskScore were selected as the independent prognostic factors (Fig. 8B). A nomogram for forecasting survival in patients with TNBC (1-, 3-, and 5-year survival) was constructed using cancer status, riskScore, and pathologic stage (Fig. 8C). A calibration curve was plotted, indicating the robust predictive ability of the nomogram model (Fig. 8D).

3.7. Functional enrichment and immune infiltration analyses between the two risk groups

Patients with TNBC in the two risk groups exhibited notable differences in functions such as glycolysis, DNA repair, and oxidative phosphorylation. (Fig. 9A, Supplementary T1able 2). Eight types of immune cells (aDC, Tcm, Tgd, NK cells, Tem, helper T cells, TFH,
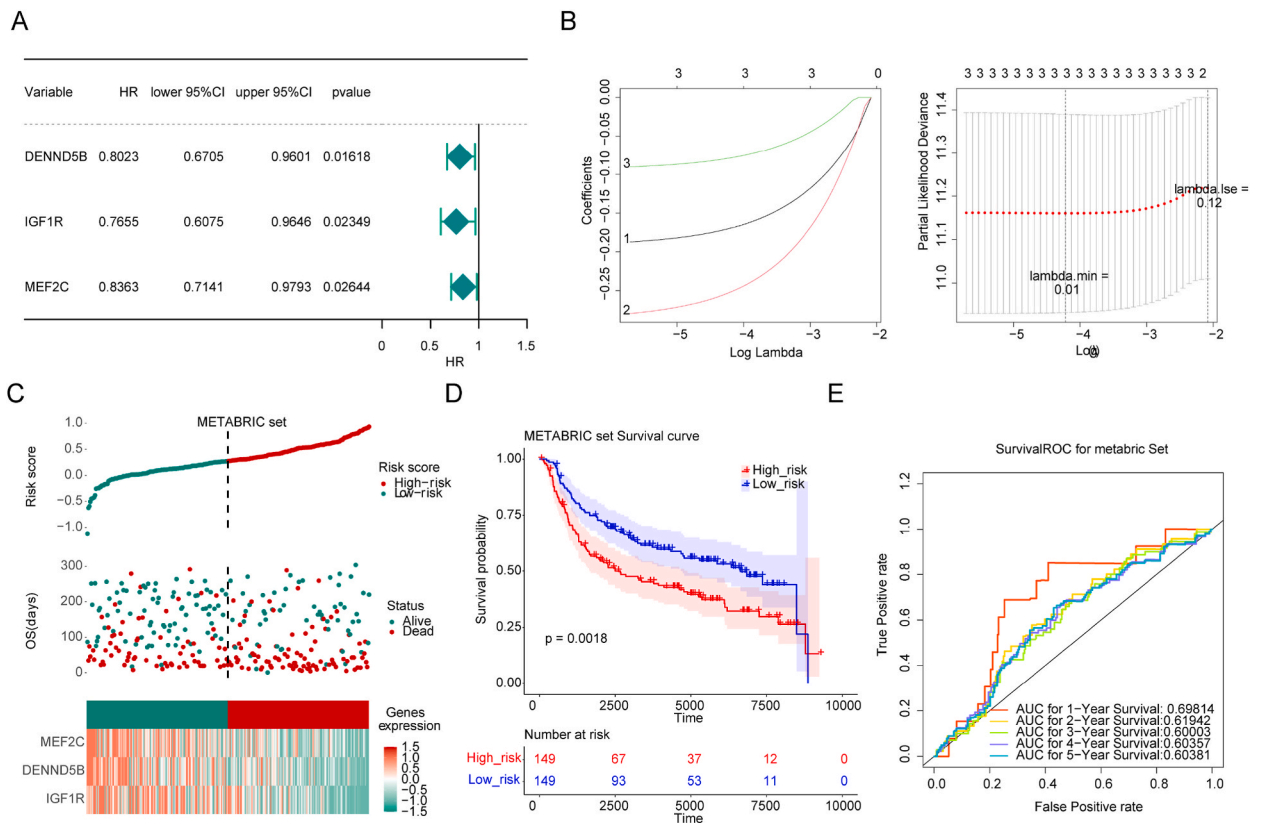
Fig. 6. Screening of biomarkers. (A) Survival-related mRNAs obtained using univariate Cox proportional hazard regression analysis. (B) Biomarkers screened out using LASSO regression analysis. (C) Risk score distribution, patient survival status, and heat map of biomarkers expressed in the METABRIC dataset. (D) K–M survival curves for the high- and low-risk groups in the METABRIC dataset. (E) ROC curves for 1–5-year survival were plotted for patients with TNBC in the METABRIC dataset.
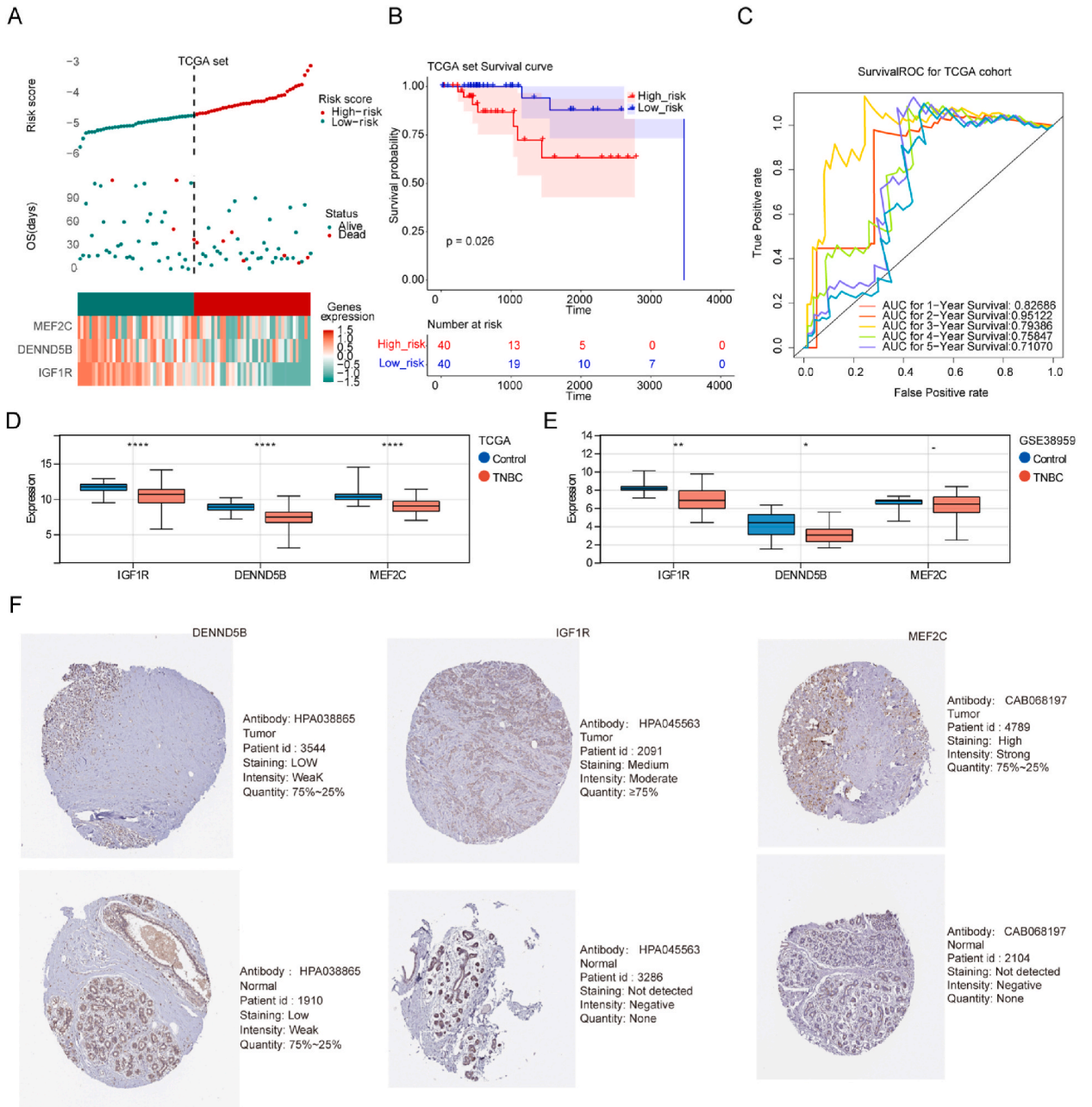
Fig. 7. Screening of biomarkers. (A) Heat map of the risk score distribution, patient survival status, and biomarkers expressed in the TCGA dataset. (B) K–M survival curves for patients with high/low-risk scores in the TCGA dataset. (C) ROC curves for 1–5-year survival for patients in the TCGA dataset. (D, E) Comparison of expression levels of three biomarkers between control samples and patients with TNBC in the TCGA and GSE38959 datasets. *p < 0.05, **p < 0.01, and ****p < 0.0001. (F) Immunohistochemistry results for the prognostic genes (biomarkers) downloaded from the Human Protein Atlas database.

and Eosinophils) displayed significant differences between the two risk groups (Fig. 9B). Moreover, the risk score exhibited a significant association with four immune cell subtypes, namely Tcm, NK cells, Tem, and eosinophils (|R| > 0.3 and p < 0.05), reflecting the key role of the immune microenvironment in TNBC (Fig. 9C).

3.8. Significance of riskScore in predicting response to immunotherapy and chemotherapy

The expression levels of LGALS9, PDCD1, and PD-L1 (CD274) were significantly different between the two risk groups (Fig. 10A). EC, AZ, and IPS were significantly different between the two risk groups (Fig. 10B, Supplementary T1able 3). IC50 values of the three
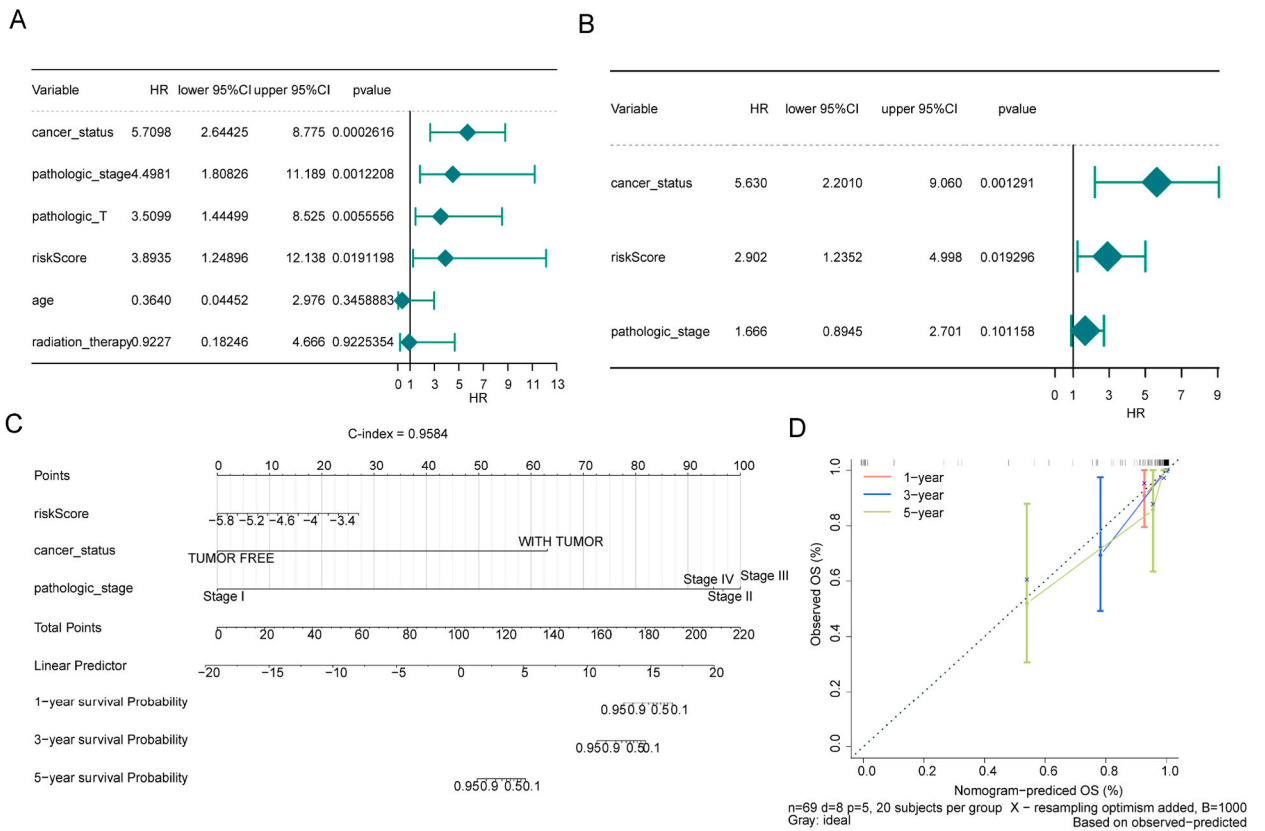
Fig. 8. Independent prognostic analysis of the risk model. (A) Univariate COX regression-based independent prognostic analysis of the risk model (cancer status, pathologic stage, and riskScore are the independent prognostic factors; p. value < 0.05). (B) Multivariate Cox analysis performed on the independent prognostic factors. (C) Nomogram predicts the survival rates of patients with TNBC (1-,3-, and 5-year survival). (D) Calibration curve for the survival nomogram model. The dashed diagonal line represents the ideal nomogram.

common chemotherapy drugs (5-fluorouracil, docetaxel, and paclitaxel) were significantly different between the two risk groups, and patients in the high-risk group were more sensitive to these drugs compared with those in the low-risk group (Fig. 10C).

3.9. Analysis of cell subtypes and prognostic factors in TNBC using scRNA-Seq

We obtained 1191 high-quality cells (Fig. 11A) and identified 2000 genes with significantly different expression levels between cells to determine cell types (Fig. 11B). The PCA results indicated that the overall distribution of the sample cells was the same. We did not find any outlier sample, and all the p-values were less than 0.05; therefore, all core cells were analyzed (Fig. 11C) and grouped into 11 classes. The main six annotations included T cells, epithelial cells, endothelial cells, fibroblasts, monocytes, and smooth muscle cells (Fig. 11D–F). Biomarkers were highly expressed in monocytes, fibroblasts, endothelial cells, and T cells; therefore, these four cell types were considered key cells (Fig. 12A). Fibroblast was different into monocytes and T cells (Fig. 12B). DENND5B was highly expressed in pseudotime 10–20, and IGF1R had a higher expression in pseudotime 0–10. In addition, MEF2C was highly expressed in pseudotime 0–25 (Fig. 12C). The heat map shows the top 25 differences in the TF activity across different cell types, and these TFs may affect the development of TNBC. TBX21 had a higher expression in T cells, and LYL1 was highly expressed in T cells and monocytes (Fig. 12D).

4. Discussion

TNBC represents a poorly defined breast cancer subtype characterized by an aggressive clinical course. CRGs influence the clinicopathologic characteristics, prognosis, and tumor microenvironment and show a significant association with tumor immunity in TNBC [9]. A six-gene risk model demonstrated effective prognostic prediction for patients with TNBC [10]. Nonetheless, the biological functions and prognostic significance of cuproptosis-related miRNAs and the target genes regulated by them have not been reported.

In our study, we obtained five survival-related and prognostic miRNAs (MIMAT0000617, MIMAT0003260, MIMAT0000758, MIMAT0005933, and MIMAT0000264). Low miR-200c expression was linked to poor survival in patients with breast cancer, and abnormal expression of miR-200c triggered apoptosis (indicated by increased cellular cAMP levels) [23]. MiR-592 played a suppressive role in breast cancer by targeting TGFβ-2, indicating its potential as a novel therapeutic target [24]. The prioritized gene list
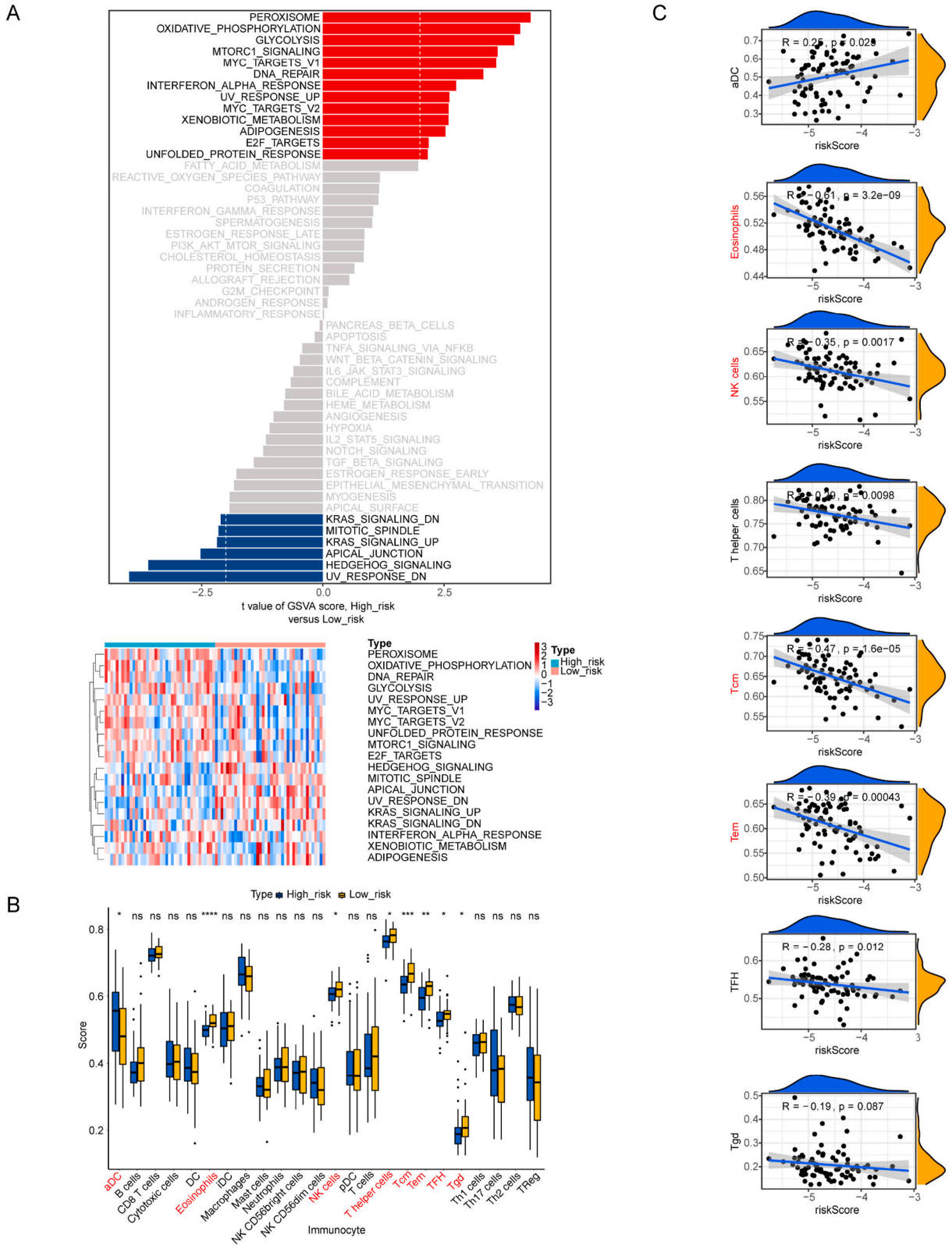
Fig. 9. Functional enrichment and immune infiltration analyses. (A) Analysis of biological signaling pathways in the high- and low-risk groups. (B) Analysis of the differences in the immune cell infiltration between the two risk groups. ns, not significant, *p < 0.05, **p < 0.01, ***p < 0.001, and ****p < 0.0001. (C) Association between immune cell subtypes and riskScore.
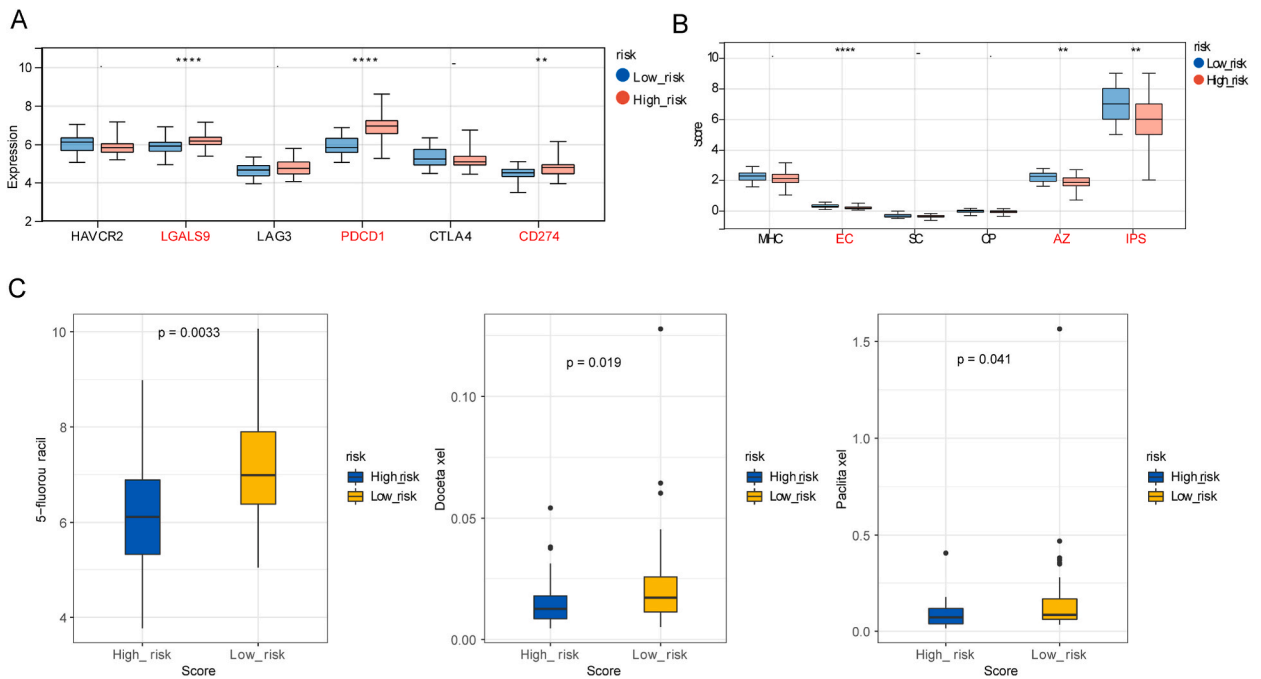
Fig. 10. Significance of riskScore in predicting response to immunotherapy and chemotherapy. (A) Expression levels of immune checkpoint genes between the two risk groups in the GSE157284 dataset. **$p < 0.01$ and ****$p < 0.0001$. (B) Comparison of IPSs (including the expression of SC, EC, MHC, and CP) for patients with TNBC. **$p < 0.01$ and ****$p < 0.0001$. (C) Comparison of the IC50 values of three chemotherapy drugs (5-fluorouracil, docetaxel, and paclitaxel) between the two risk groups.

based on the robust rank aggregation method indicated the upregulation of miR-135b-5p. The target genes modulated by miR-135b-5p exhibited association with processes, such as the regulation of transcription, DNA-dependent, and signal transduction. Notably, these processes have been implicated in the progression of TNBC [25]. Upregulated miR-1277–3p is involved in various autism spectrum disorder-related pathways associated with cell signaling, cell adhesion, and cancer metabolism [26]. The oncogenesis and development of breast cancer may be enhanced by miR-203a-3p [27]. Similar to those of previous studies, our findings indicated that MIMAT0000264 exhibited heightened expression in the high-risk group (HR $>$ 1), whereas the expression of MIMAT0000617 and MIMAT0003260 was elevated in the low-risk group compared to the high-risk group. However, the expression of MIMAT0000758 and MIMAT0005933 was higher in the low-risk group compared to the high-risk group, and these findings were different from those of previous reports. These two miRNAs may contribute to the regulation of breast cancer pathogenesis through involvement in multiple tumor-related pathways.

In addition, we identified three biomarkers (DENND5B, IGF1R, and MEF2C). DENND5B is a guanine nucleotide exchange factor that activates RAB39A and RAB39B. It has been recognized as one of the 13 loci significantly linked to the risk of colorectal cancer in Asia [28]; however, its relationship with TNBC has not been confirmed. We explored the role of DENND5B in the progression of TNBC. IGF-1R is a transmembrane receptor, belonging to the class of tyrosine kinase receptors. This receptor facilitates the binding to IGF-1, a polypeptide protein hormone that shares a similar molecular structure with insulin. In the current study, 75% of patients with breast cancer showed the activation of the insulin/IGF-1R signaling pathway. This signal transduction axis is related to the increase in cancer progression, angiogenesis, and metastasis [29]. The IGF signal axis is implicated in TNBC, and the IGF gene signature is upregulated in TNBC and TNBC cell lines. The IGF signaling pathway promotes the survival and proliferation of TNBC cells. The downregulation of the IGF-1R signaling pathway enhances the IGF-II/IR-A signaling pathway, thereby promoting the typical Wnt signaling pathway [30]. Myocyte enhancer factor 2 (MEF2)C is an important transcription factor of the MEF2 family. This transcription factor is crucial in many developmental processes. Its deregulation impacts cell differentiation, eventually resulting in heightened cell proliferation (particularly important in cancer). MEF2C plays an important regulatory role in Ca2+, mitogen-activated protein kinase, Wnt, and phosphatidylinositol 3-kinase/protein kinase B (Akt) signaling pathways through direct interactions with effector proteins. Notably, MEF2C silencing can significantly reduce TNBC cell migration [31]. Integrating findings from functional enrichment analysis, it is inferred that these three genes could be involved in the onset and progression of TNBC via the Wnt signaling pathway.

This research revealed notable differences in patient prognoses between the two risk groups, with the high-risk group experiencing poorer outcomes. Through functional enrichment analysis, significant variations were noted between the two risk groups in three key functions: oxidative phosphorylation, DNA repair, and glycolysis. Oxidative phosphorylation represents a metabolic susceptibility in chemotherapy-resistant TNBC [32]. Copper depletion modulates mitochondrial oxidative phosphorylation to impair TNBC metastasis [33]. MYC and MCL1 cooperate to maintain chemotherapy-resistant cancer stem cells in TNBC by regulating mitochondrial oxidative phosphorylation and ROS generation [34]. Most cases of TNBC have a DNA repair deficiency that can be identified using mutational
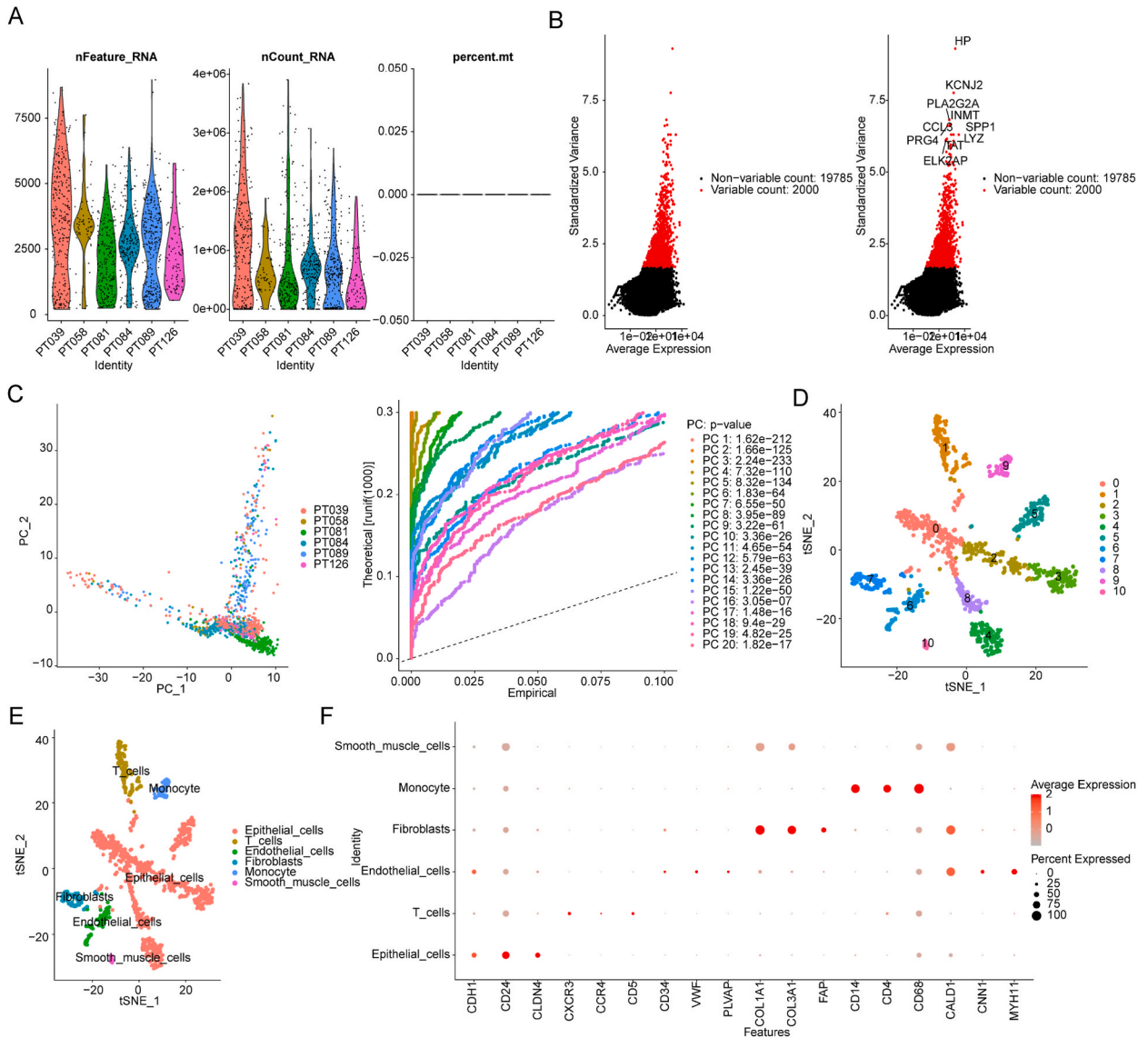
Fig. 11. Expression of cell subtypes and prognostic genes in TNBC. (A) Violin plot screens high-quality cells in the GSE118389 dataset. Gene expression levels are normalized using a linear regression model. (B) Identification of highly variable gene expression in core cells. (C) Overall distribution of the sample cells using the JackStraw and ScoreJackStraw functions for PCA. (D, E) tSNE plot shows the clustering results for core cells. Each point represents a single cell, colored according to cell type. The cells were clustered into six distinct types. (F) Expression profile of the prognostic genes based on the cell cluster.

signature analysis and can be targeted with PARP inhibitors [35]. Studies on loss and gain of function demonstrated that FZD5 assisted DNA damage repair in TNBC [36]. Myeloid-derived suppressor cells (MDSCs) and tumor immunity are regulated by aerobic glycolysis through a specific CEBPB isoform in TNBC [37]. Overall, these three functions are associated with the prognosis and treatment of TNBC.

Significant differences were observed between the two risk groups in eight types of immune cells (aDC, Tcm, Tgd, NK cells, Tem, helper T cells, TFH, and eosinophils). The purified naive Tcm and Tscm cell subsets exhibited enhanced persistence and antitumor immunity when compared to ACT populations comprising Teff and Tem cells [38]. Lu et al. identified an association between PRR7-AS1 expression and various immune cell types, including T helper cells, macrophages, NK CD56 [bright] cells, TFH cells, Th2 cells, Th1 cells, aDC cells, cytotoxic cells, DC cells, neutrophils, Tgd cells, and Th17 cells, suggesting that PRR7-AS1 might be a potential prognostic biomarker for patients with hepatocellular carcinoma [39]. We speculate that these cells have similar effects on the development of TNBC; however, further studies are needed. Hollern et al. [40] reported that immune checkpoint therapy induces the activation of Tfh cells, which activate B cells to promote antitumor responses in mouse models of TNBC. The authors identified a novel biomarker for immune checkpoint therapy and demonstrated B-cell-mediated activation of T cells and antibody production in response
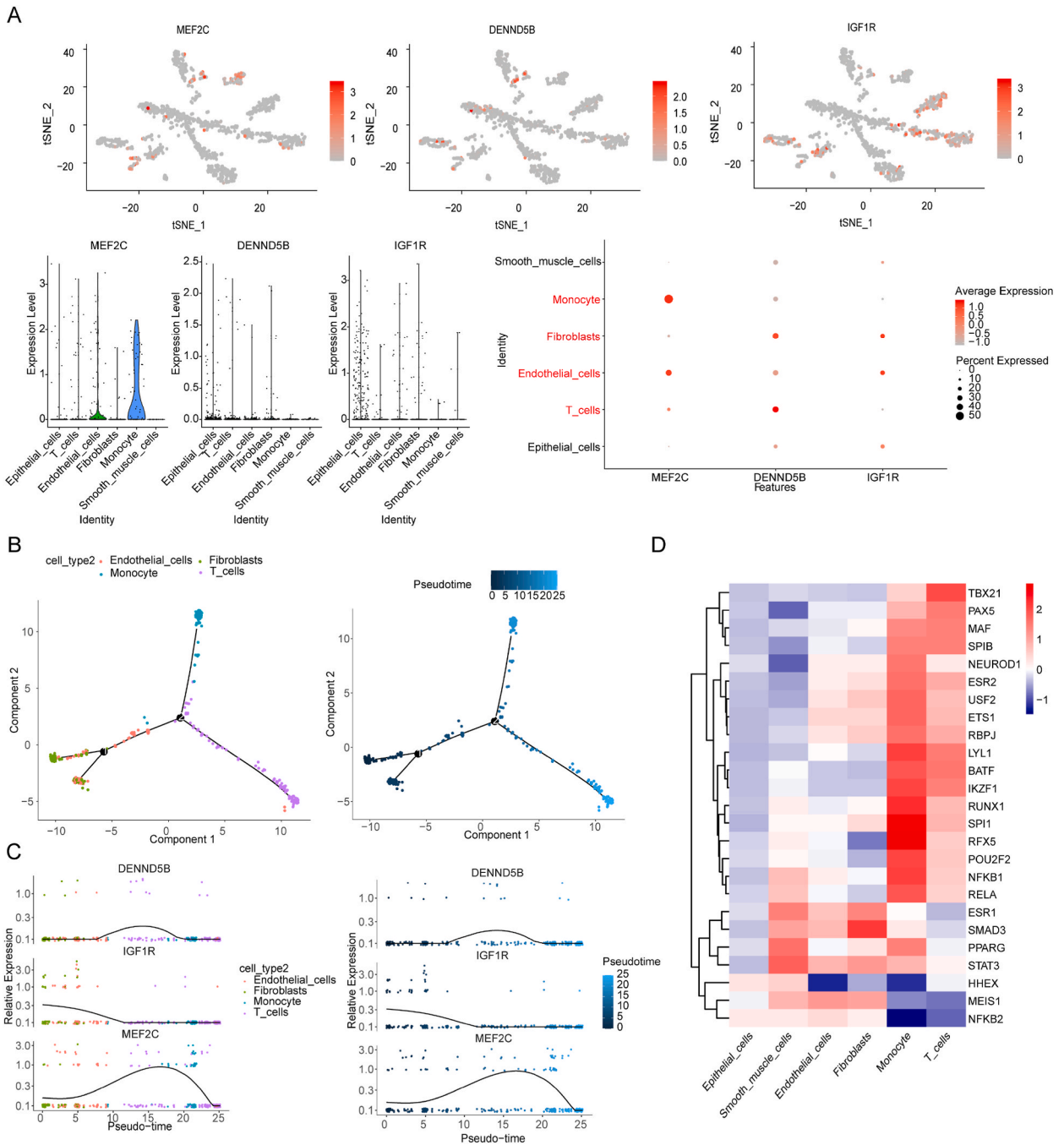
Fig. 12. Analysis of cell subtypes and prognostic factors in TNBC. (A) Analysis for the trajectory-dependent expression of biomarkers and its linear differentiation. (B) Pseudochronologic analysis trajectories of the prognostic genes in different cell types inferred using Monocle2; each point corresponds to a cell. (C) Analysis of the relative expression of DENND5B, IGF1R, and MEF2C in Pseudotime. (D) Heat map shows the TFs with significant differences between cell populations.

to immunotherapy. Boieri et al. [41] demonstrated the critical role of CD4$^+$ Th2 cells in the immune response against breast cancer. They highlighted the terminal differentiation of CD4$^+$ Th2 cells as a distinctive effector mechanism for both cancer immunoprevention and therapy. Additionally, the direct antitumor effects were attributed to the targeting of high-affinity NK cells towards PD-L1, which resulted in the targeting of suppressive MDSC populations [42]. Manoochehri et al. reported an association between TNBC and alterations in the ratios or proportions of various leukocyte subtypes. Notably, a significant association was observed between TNBC and decreased NK cell counts, indicating the strongest correlation of NK cells with TNBC among the examined leukocyte populations [43].

Functional T follicular regulatory (Tfr) cells inhibited the activities of functional Tfh cells through a mechanism involving the glycoprotein A repetitions predominant (GARP) receptor and TGF-β. This inhibitory mechanism was dependent on the presence of TGF-β and mediated by the association of GARP with TGF-β. The balance between functional Tfh tumor-infiltrating lymphocytes (TILs) and functional Tfr TILs controlled the activity of tumor-associated TLS [44]. Grisaru-Tal et al. [45] identified a mechanism through which the tumor microenvironment instructs eosinophils to acquire antitumorigenic properties. This significant finding opens up the potential for the development of approaches that specifically target eosinophils for anticancer therapies. Overall, these findings enhance our understanding of the immune system functioning and cuproptosis-related immune cells in TNBC, and immune cell concentrations can be potentially used as a non-invasive marker for evaluating TNBC risk, facilitating detection, and implementing preventive measures.

Our findings indicated elevated expression levels of three target genes in four key cells, namely monocytes, T cells, endothelial cells, and fibroblasts. Wu et al. calculated the TIL score using the xCell algorithm. Scores reached their peak in the TNBC subtype and were at their lowest in the ER-positive/HER2-negative subtypes. This phenomenon was related to monocyte infiltration [46]. TNBC showed heterogeneity between and within tumors, and tumor-related fibroblasts were one of the sources of this heterogeneity [47]. Wang et al. found that fibroblasts can induce the formation of lipid-related macrophages, mediate immunosuppression, and participate in promoting immune escape in TNBC [48]. Zhou et al. confirmed that extracellular adenosine triphosphate treatment increased the expression of connective tissue growth factor (CTGF) in TNBC cells and endothelial cells by upregulating integrin β1 expression in TNBC cells. VCAM-1 in endothelial cells stimulates TNBC cells to adhere to endothelial cells and mediates the migration of TNBC cells through the endothelial cell layer (mediated by CTGF) [49]. Regulatory T cells (Treg) are enriched in TNBC tissues, $CD8^+$ T cells are depleted, and some cytotoxic $CD8^+$ T cells are in a state of transition to failure, indicating that their tumor-toxic activity is inhibited [50]. These cells may be targeted for the treatment of TNBC.

Immunotherapy is the most popular treatment for malignant tumors, often regarded as the fifth fundamental modality in cancer management, along with targeted therapy, radiotherapy, chemotherapy, and surgery [51]. Immune checkpoints are the molecular structures on the surface of tumor cells or in the tumor microenvironment, which regulate the activity and function of immune cells to protect tumor cells from the immune system. Immune checkpoint molecules mainly include CTLA-4, PD-L1, and PD-1 [52]. They are located on the surface of T cells and tumor cells. These molecules can inhibit the activity of T cells through specific binding interactions [53]. IPS, a system grounded in machine learning techniques, computes z-scores utilizing data from four cell types linked to immunogenicity. According to their median risk score, Li et al. categorized patients with breast cancer into groups of high and low risk. Patients with low risk exhibited a superior immune response and a higher presence of antitumor immune infiltrating cells compared to those in the high-risk category [54]. In our study, the inhibitory concentrations of three chemotherapy drugs (5-fluorouracil, docetaxel, and paclitaxel) were significantly different between the two risk groups. Our findings indicate an increased sensitivity to certain drugs among TNBC patients classified in the high-risk group. RBP7 may be used as a tumor microenvironment regulator to induce 5-fluorouracil resistance, affecting the prognosis of patients with colorectal cancer [55]. Docetaxel activates the antitumor immune response in a CGA/STING-dependent manner and promotes T-cell infiltration. The combination of immunotherapy with docetaxel may improve the clinical benefits of immunotherapy [56]. In addition, the cell death index (CDI) showed a correlation with key tumor microenvironment components and immune checkpoint genes. Patients exhibiting a high CDI demonstrated resistance to standard adjuvant chemotherapy (e.g., oxaliplatin and docetaxel) [57]. Paclitaxel acts by directly eliminating tumor cells and modulating a range of immune cells [58]. Paclitaxel contributes to the reduction of Treg cells, aids in the production of interleukin-10, alters growth factors via Tregs, and enhances antigen presentation mediated by DCs [59]. Therefore, these three drugs can be used in the treatment of TNBC; however, their therapeutic effect and clinincal use need to be verified.

We found five prognostic miRNAs (MIMAT0000617, MIMAT0003260, MIMAT0000758, MIMAT0005933, and MIMAT0000264) and three prognostic genes (DENND5B, IGF1R, and MEF2C). Moreover, we developed a novel prognostic model for patients with TNBC, unveiled new candidates as prognostic markers and therapeutic targets for the management of the disease, and revealed that cuproptosis is closely related to TNBC tumors. Although our results did not directly elaborate on the mechanism of cuproptosis, we discussed the biological functions of cuproptosis-related miRNAs and their target genes for the first time. We conducted a quantitative assessment of the expression levels of prognostic genes and the clinical features of patients to ascertain their survival rates. The construction of the TNBC prognostic model may help predict the treatment response and survival time of patients to make individualized treatment decisions and improve the overall treatment efficacy. However, the use of prognostic models still needs to be verified clinically.

5. Conclusions

In this study, we pioneered the investigation into miRNAs linked to the prognosis of patients with TNBC. Subsequently, we integrated these miRNAs with their target genes to develop a risk model, enabling the assessment of patient prognosis. We screened five predictive miRNAs (miR-203a-3p, miR-1277–3p, miR-200c-3p, miR-135b-5p, and miR-592) and three biomarkers (DENND5B, IGF1R, and MEF2C) for patients with TNBC by analyzing the transcriptome data, single-cell data, and miRNA information. The outcomes of our study will establish a theoretical foundation for the assessment of copper-mediated death's role in TNBC in subsequent research endeavors. In addition, our findings indicated a novel target for enhancing the prognosis and treatment of patients with TNBC. Nevertheless, this study has some limitations. Firstly, the analysis in this study relied on a restricted number of samples from the public database, and the clinical sample size should be expanded. In addition, it is important to further verify these findings in cell or animal models, which is our next research focus. In addition, we will continue to focus on the role of prognosis-related miRNAs and target genes in TNBC and further explore their mechanism of action.

The following supporting information can be found in the zip file. Table S1: Correlation of the CRG score to DE-miRNAs; Table S2: Hallmarkpathways with significant differences between the high- and low-risk groups; Table S3: IPSscore of samples in the GSE157284 dataset.

Data availability statement

The datasets analyzed in this study were collected from the TCGA (https://portal.gdc.cancer.gov/), METABRIC (https://www.mercuriolab.umassmed.edu/metabric), and GEO (https://www.ncbi.nlm.nih.gov/geo/) databases. The names of the datasets are detailed in the Materials and Methods section, and the raw data can be obtained from the corresponding author.

Thanks: We thank Bullet Edits Limited for the linguistic editing and proofreading of the manuscript.

We had uploaded the data and images to MENDELEY.

CRediT authorship contribution statement

Yitao Wang: Writing – review & editing, Writing – original draft, Formal analysis. **Jundan Wang:** Resources, Data curation. **Jing Jiang:** Software, Methodology. **Wei Zhang:** Investigation. **Long Sun:** Supervision, Software. **Qidong Ge:** Visualization. **Chao Li:** Project administration, Methodology. **Xinlin Li:** Validation. **Xujun Li:** Funding acquisition. **Shenghong Shi:** Writing – review & editing, Project administration, Methodology, Conceptualization.

Declaration of competing interest

The authors declare that they have no known competing financial interests or personal relationships that could have appeared to influence the work reported in this paper.

References

[1] D. Trapani, O. Ginsburg, T. Fadelu, N.U. Lin, M. Hassett, A.M. Ilbawi, et al., Global challenges and policy solutions in breast cancer control, Cancer Treat Rev. 104 (2022) 102339, https://doi.org/10.1016/j.ctrv.2022.102339.

[2] R. Dent, M. Trudeau, K.I. Pritchard, W.M. Hanna, H.K. Kahn, C.A. Sawka, et al., Triple-negative breast cancer: clinical features and patterns of recurrence, Clin. Cancer Res. 13 (2007) 4429–4434, https://doi.org/10.1158/1078-0432.CCR-06-3045.

[3] N. Garmpis, C. Damaskos, A. Garmpi, K. Nikolettos, D. Dimitroulis, E. Diamantis, et al., Molecular classification and future therapeutic challenges of triple-negative breast cancer, In Vivo 34 (2020) 1715–1727, https://doi.org/10.21873/invivo.11965.

[4] Y. Fu, L. Chen, C. Chen, Y. Ge, M. Kang, Z. Song, et al., Crosstalk between alternative polyadenylation and miRNAs in the regulation of protein translational efficiency, Genome Res. 28 (2018) 1656–1663, https://doi.org/10.1101/gr.231506.117.

[5] Y.L. Wang, R.H. Liang, C.Y. Wang, R.P. Zhang, S.Y. Wu, X. Han, et al., MicroRNA-543 inhibits the proliferation, migration, invasion, and epithelial-mesenchymal transition of triple-negative breast cancer cells via down-regulation of ACTL6A gene, Clin. Transl. Oncol. 24 (2021) 84–92, https://doi.org/10.1007/s12094-021-02672-z.

[6] L.L. Chen, Z.J. Zhang, Z.B. Yi, J.J. Li, MicroRNA-211-5p suppresses tumour cell proliferation, invasion, migration and metastasis in triple-negative breast cancer by directly targeting SETBP1, Br. J. Cancer 117 (2017) 78–88, https://doi.org/10.1038/bjc.2017.150.

[7] T. Furukawa, M. Komatsu, R. Ikeda, K. Tsujikawa, S. Akiyama, Copper transport systems are involved in multidrug resistance and drug transport, Curr. Med. Chem. 15 (2008) 3268–3278, https://doi.org/10.2174/092986708786848479.

[8] L. Chen, J. Min, F. Wang, Copper homeostasis and cuproptosis in health and disease, Signal Transduct. Targeted Ther. 7 (2022) 378, https://doi.org/10.1038/s41392-022-01229-y.

[9] S. Sha, L. Si, X. Wu, Y. Chen, H. Xiong, Y. Xu, et al., Prognostic analysis of cuproptosis-related gene in triple-negative breast cancer, Front. Immunol. 13 (2022) 922780, https://doi.org/10.3389/fimmu.2022.922780.

[10] B. Zhu, S. Wang, R. Wang, X. Wang, Identification of molecular subtypes and a six-gene risk model related to cuproptosis for triple negative breast cancer, Front. Genet. 13 (2022) 1022236, https://doi.org/10.3389/fgene.2022.1022236.

[11] B. Shi, W. Zhang, T. Wang, Z. Cui, The therapeutic and prognostic role of cuproptosis-related genes in triple negative breast cancer, BMC Bioinf. 24 (2023) 223, https://doi.org/10.1186/s12859-023-05348-3.

[12] C. Gao, N. Kong, F. Zhang, L. Zhou, M. Xu, L. Wu, Development and validation of the potential biomarkers based on m6A-related lncRNAs for the predictions of overall survival in the lung adenocarcinoma and differential analysis with cuproptosis, BMC Bioinf. 23 (2022) 327, https://doi.org/10.1186/s12859-022-04869-7.

[13] E.V. Polishchuk, A. Merolla, J. Lichtmannegger, A. Romano, A. Indrieri, E.Y. Ilyechova, et al., Activation of Autophagy, observed in Liver tissues from patients with Wilson disease and from ATP7B-deficient animals, protects Hepatocytes from copper-Induced apoptosis, Gastroenterology 156 (2019) 1173–1189 e5, https://doi.org/10.1053/j.gastro.2018.11.032.

[14] S. Sun, Cj, Q. Yang, S. Zhao, Z. Wang, The association between copper transporters and the prognosis of cancer patients undergoing chemotherapy a meta-analysis of literatures and datasets, Oncotarget 8 (2017) 16036–16051, https://doi.org/10.18632/oncotarget.13917.

[15] F. Wang, H. Lin, Q. Su, C. Li, Cuproptosis-related lncRNA predict prognosis and immune response of lung adenocarcinoma, World J. Surg. Oncol. 20 (2022) 275, https://doi.org/10.1186/s12957-022-02727-7.

[16] A. Mayakonda, D.C. Lin, Y. Assenov, C. Plass, H.P. Koeffler, Maftools: efficient and comprehensive analysis of somatic variants in cancer, Genome Res. 28 (2018) 1747–1756, https://doi.org/10.1101/gr.239244.118.

[17] H. Zhang, Mp, S. Davis, RCircos: an R package for Circos 2D track plots, BMC Bioinf. 14 (2013) 244, https://doi.org/10.1186/1471-2105-14-244.

[18] M.E. Ritchie, B. Phipson, D. Wu, Y. Hu, C.W. Law, W. Shi, et al., Limma powers differential expression analyses for RNA-sequencing and microarray studies, Nucleic Acids Res. 43 (2015) e47, https://doi.org/10.1093/nar/gkv007.

[19] T. Mosmann, Rapid colorimetric assay for cellular growth and survival application to proliferation and cytotoxicity assays, J. Immunol. Methods 65 (1983) 55–63, https://doi.org/10.1016/0022-1759(83)90303-4.

[20] T. Wu, E. Hu, S. Xu, M. Chen, P. Guo, Z. Dai, et al., clusterProfiler 4.0: a universal enrichment tool for interpreting omics data, Innovation 2 (2021) 100141, https://doi.org/10.1016/j.xinn.2021.100141.

[21] P. Charoentong, F. Finotello, M. Angelova, C. Mayer, M. Efremova, D. Rieder, et al., Pan-cancer Immunogenomic analyses reveal Genotype-Immunophenotype relationships and Predictors of response to checkpoint Blockade, Cell Rep. 18 (2017) 248–262, https://doi.org/10.1016/j.celrep.2016.12.019.

[22] A.A. Hakimi, E. Reznik, C.H. Lee, C.J. Creighton, A.R. Brannon, A. Luna, et al., An integrated metabolic atlas of Clear cell Renal cell carcinoma, Cancer Cell 29 (2016) 104–116, https://doi.org/10.1016/j.ccell.2015.12.004.

[23] D.D. Zhang, Y. Li, Y. Xu, J. Kim, S. Huang, Phosphodiesterase 7B/microRNA-200c relationship regulates triple-negative breast cancer cell growth, Oncogene 38 (2019) 1106–1120, https://doi.org/10.1038/s41388-018-0499-2.

[24] W. Hou, H. Zhang, X. Bai, X. Liu, Y. Yu, L. Song, et al., Suppressive role of miR-592 in breast cancer by repressing TGF-beta2, Oncol. Rep. 38 (2017) 3447–3454, https://doi.org/10.3892/or.2017.6029.

[25] L.D. Naorem, M. Muthaiyan, A. Venkatesan, Identification of dysregulated miRNAs in triple negative breast cancer: a meta-analysis approach, J. Cell. Physiol. 234 (2018) 11768–11779, https://doi.org/10.1002/jcp.27839.

[26] Z.X. Huang, Y. Chen, H.R. Guo, G.F. Chen, Systematic review and bioinformatic analysis of microRNA expression in autism spectrum disorder Identifies pathways associated with cancer, metabolism, cell signaling, and cell adhesion, Front. Psychiatr. 12 (2021) 630876, https://doi.org/10.3389/fpsyt.2021.630876.

[27] K.T. Cai, C.X. Feng, J.C. Zhao, R.Q. He, J. Ma, J.C. Zhong, Upregulated miR-203a-3p and its potential molecular mechanism in breast cancer: a study based on bioinformatics analyses and a comprehensive meta-analysis, Mol. Med. Rep. 18 (2018) 4994–5008, https://doi.org/10.3892/mmr.2018.9543.

[28] S.A. Jeon, Y.J. Ha, J.H. Kim, J.H. Kim, S.K. Kim, Y.S. Kim, et al., Genomic and transcriptomic analysis of Korean colorectal cancer patients, Genes Genomics 44 (2022) 967–979, https://doi.org/10.1007/s13258-022-01275-4.

[29] J. Li, E.L.K. Goh, J. He, Y. Li, Z. Fan, Z. Yu, et al., Emerging Intrinsic therapeutic targets for metastatic breast cancer, Biology 12 (2023) 697, https://doi.org/10.3390/biology12050697.

[30] L.M. Rota, L. Albanito, M.E. Shin, C.L. Goyeneche, S. Shushanov, E.J. Gallagher, et al., IGF1R inhibition in mammary epithelia promotes canonical Wnt signaling and Wnt1-driven tumors, Cancer Res. 74 (2014) 5668–5679, https://doi.org/10.1158/0008-5472.CAN-14-0970.

[31] S. Caetano, A.R. Garcia, I. Figueira, M.A. Brito, MEF2C and miR-194-5p: new Players in triple negative breast cancer Tumorigenesis, Int. J. Mol. Sci. 24 (2023) 14297, https://doi.org/10.3390/ijms241814297.

[32] K.W. Evans, E. Yuca, S.S. Scott, M. Zhao, N. Paez Arango, C.X. Cruz Pico, et al., Oxidative phosphorylation is a metabolic Vulnerability in chemotherapy-resistant triple-negative breast cancer, Cancer Res. 81 (2021) 5572–5581, https://doi.org/10.1158/0008-5472.CAN-20-3242.

[33] D. Ramchandani, M. Berisa, D.A. Tavarez, Z. Li, M. Miele, Y. Bai, et al., Copper depletion modulates mitochondrial oxidative phosphorylation to impair triple negative breast cancer metastasis, Nat. Commun. 12 (2021) 7311, https://doi.org/10.1038/s41467-021-27559-z.

[34] K.M. Lee, J.M. Giltnane, J.M. Balko, L.J. Schwarz, A.L. Guerrero-Zotano, K.E. Hutchinson, et al., MYC and MCL1 Cooperatively promote chemotherapy-resistant breast cancer stem cells via regulation of mitochondrial oxidative phosphorylation, Cell Metabol. 26 (2017) 633–647 e7, https://doi.org/10.1016/j.cmet.2017.09.009.

[35] N. Chopra, H. Tovey, A. Pearson, R. Cutts, C. Toms, P. Proszek, et al., Homologous recombination DNA repair deficiency and PARP inhibition activity in primary triple negative breast cancer, Nat. Commun. 11 (2020) 2662, https://doi.org/10.1038/s41467-020-16142-7.

[36] Y. Sun, Z. Wang, L. Na, D. Dong, W. Wang, C. Zhao, FZD5 contributes to TNBC proliferation, DNA damage repair and stemness, Cell Death Dis. 11 (2020) 1060, https://doi.org/10.1038/s41419-020-03282-3.

[37] T. Xu, J. Liu, Y. Xia, Z. Wang, X. Li, Q. Gao, Integrated analysis reveals the participation of IL4I1, ITGB7, and FUT7 in reshaping the TNBC immune microenvironment by targeting glycolysis, Ann. Med. 53 (2021) 916–928, https://doi.org/10.1080/07853890.2021.1937694.

[38] Q. Liu, Z. Sun, L. Chen, Memory T cells: strategies for optimizing tumor immunotherapy, Protein Cell 11 (2020) 549–564, https://doi.org/10.1007/s13238-020-00707-9.

[39] Y. Lu, S. Chen, Q. Wang, J. Zhang, X. Pei, PRR7-AS1 Correlates with immune cell infiltration and is a diagnostic and prognostic marker for hepatocellular carcinoma, JAMA Oncol. 2022 (2022) 1939368, https://doi.org/10.1155/2022/1939368.

[40] D.P. Hollern, N. Xu, A. Thennavan, C. Glodowski, S. Garcia-Recio, K.R. Mott, et al., B cells and T follicular helper cells mediate response to checkpoint inhibitors in high mutation Burden mouse models of breast cancer, Cell 179 (2019) 1191–1206 e21, https://doi.org/10.1016/j.cell.2019.10.028.

[41] M. Boieri, A. Malishkevich, R. Guennoun, E. Marchese, S. Kroon, K.E. Trerice, et al., CD4+ T helper 2 cells suppress breast cancer by inducing terminal differentiation, J. Exp. Med. 219 (2022) e20201963, https://doi.org/10.1084/jem.20201963.

[42] K.P. Fabian, M.R. Padget, R.N. Donahue, K. Solocinski, Y. Robbins, C.T. Allen, et al., PD-L1 targeting high-affinity NK (t-haNK) cells induce direct antitumor effects and target suppressive MDSC populations, J Immunother Cancer 8 (2020) e000450, https://doi.org/10.1136/jitc-2019-000450.

[43] M. Manoochehri, T. Hielscher, N. Borhani, C. Gerhauser, O. Fletcher, A.J. Swerdlow, et al., Epigenetic quantification of circulating immune cells in peripheral blood of triple-negative breast cancer patients, Clin. Epigenet. 13 (2021) 207, https://doi.org/10.1186/s13148-021-01196-1.

[44] G. Noel, M.L. Fontsa, S. Garaud, P. De Silva, A. de Wind, G.G. Van den Eynden, et al., Functional Th1-oriented T follicular helper cells that infiltrate human breast cancer promote effective adaptive immunity, J. Clin. Invest. 131 (2021) e139905, https://doi.org/10.1172/JCI139905.

[45] S. Grisaru-Tal, S. Dulberg, L. Beck, C. Zhang, M. Itan, S. Hediyeh-Zadeh, et al., Metastasis-entrained eosinophils enhance Lymphocyte-mediated antitumor immunity, Cancer Res. 81 (2021) 5555–5571, https://doi.org/10.1158/0008-5472.CAN-21-0839.

[46] R. Wu, M. Oshi, M. Asaoka, L. Yan, M.G.K. Benesch, T. Khoury, et al., Intratumoral tumor infiltrating lymphocytes (TILs) are associated with cell proliferation and Better survival but not Always with chemotherapy response in breast cancer, Ann. Surg. 278 (2023) 587–597, https://doi.org/10.1097/SLA.0000000000005954.

[47] X. Wu, Lw, W. Zhang, D. Zhang, H. Mei, M. Zhang, Y. Cui, Z. Zhuo, Integrated analysis of single-cell RNA-seq and bulk RNA-seq unravels the heterogeneity of cancer-associated fibroblasts in TNBC, Aging (Albany NY) 5 (2022) 12674–12697, https://doi.org/10.18632/aging.205205.

[48] G. Wang, H. Zhang, X. Shen, W. Jin, X. Wang, Z. Zhou, Characterization of cancer-associated fibroblasts (CAFs) and development of a CAF-based risk model for triple-negative breast cancer, Cancer Cell Int. 23 (2023) 294, https://doi.org/10.1186/s12935-023-03152-w.

[49] Y.T. Zhou, Y.Q. Yu, H. Yang, H. Yang, Y.F. Huo, Y. Huang, et al., Extracellular ATP promotes angiogenesis and adhesion of TNBC cells to endothelial cells via upregulation of CTGF, Cancer Sci. 113 (2022) 2457–2471, https://doi.org/10.1111/cas.15375.

[50] S. Ding, N. Qiao, Q. Zhu, Y. Tong, S. Wang, X. Chen, et al., Single-cell atlas reveals a distinct immune profile fostered by T cell-B cell crosstalk in triple negative breast cancer, Cancer Commun. 43 (2023) 661–684, https://doi.org/10.1002/cac2.12429.

[51] C. Luo, P. Wang, S. He, J. Zhu, Y. Shi, J. Wang, Progress and Prospect of immunotherapy for triple-negative breast cancer, Front. Oncol. 12 (2022) 919072, https://doi.org/10.3389/fonc.2022.919072.

[52] S.J. Wang, S.K. Dougan, M. Dougan, Immune mechanisms of toxicity from checkpoint inhibitors, Trends Cancer 9 (2023) 543–553, https://doi.org/10.1016/j.trecan.2023.04.002.

[53] J.B. Haanen, C. Robert, Immune checkpoint inhibitors, Prog Tumor Res. 42 (2015) 55–66, https://doi.org/10.1159/000437178.

[54] J. Li, H. Qiao, F. Wu, S. Sun, C. Feng, C. Li, et al., A novel hypoxia- and lactate metabolism-related signature to predict prognosis and immunotherapy responses for breast cancer by integrating machine learning and bioinformatic analyses, Front. Immunol. 13 (2022) 998140, https://doi.org/10.3389/fimmu.2022.998140.

[55] X. Huang, K. Ke, W. Jin, Q. Zhu, Q. Zhu, R. Mei, et al., Identification of genes related to 5-fluorouracil based chemotherapy for colorectal cancer, Front. Immunol. 13 (2022) 887048, https://doi.org/10.3389/fimmu.2022.887048.

[56] Z. Ma, W. Zhang, B. Dong, Z. Xin, Y. Ji, R. Su, et al., Docetaxel remodels prostate cancer immune microenvironment and enhances checkpoint inhibitor-based immunotherapy, Theranostics 12 (2022) 4965–4979, https://doi.org/10.7150/thno.73152.

[57] Y. Zou, J. Xie, S. Zheng, W. Liu, Y. Tang, W. Tian, et al., Leveraging diverse cell-death patterns to predict the prognosis and drug sensitivity of triple-negative breast cancer patients after surgery, Int. J. Surg. 107 (2022) 106936, https://doi.org/10.1016/j.ijsu.2022.106936.

[58] V. Vassileva, C.J. Allen, M. Piquette-Miller, Effects of sustained and intermittent paclitaxel therapy on tumor repopulation in ovarian cancer, Mol. Cancer Therapeut. 7 (2008) 630–637, https://doi.org/10.1158/1535-7163.MCT-07-2117.

[59] K. Fukuda, T. Funakoshi, T. Sakurai, Y. Nakamura, M. Mori, K. Tanese, et al., Peptide-pulsed dendritic cell vaccine in combination with carboplatin and paclitaxel chemotherapy for stage IV melanoma, Melanoma Res. 27 (2017) 326–334, https://doi.org/10.1097/CMR.0000000000000342.